An RNA aptamer restores defective bone growth in FGFR3-related skeletal dysplasia in mice

Takeshi Kimura1†, Michaela Bosakova2,3,4†, Yosuke Nonaka5†, Eva Hruba4, Kie Yasuda1, Satoshi Futakawa5, Takuo Kubota1, Bohumil Fafilek2,3,4, Tomas Gregor2,3, Sara P. Abraham2, Regina Gomolkova2,4, Silvie Belaskova3, Martin Pesl2,3,6, Fabiana Csukasi7,8, Ivan Duran7,8, Masatoshi Fujiwara5, Michaela Kavkova9, Tomas Zikmund9, Josef Kaiser9, Marcela Buchtova4,10, Deborah Krakow7, Yoshikazu Nakamura5,11*, Keiichi Ozono1*, Pavel Krejci2,3,4*

Achondroplasia is the most prevalent genetic form of dwarfism in humans and is caused by activating mutations in FGFR3 tyrosine kinase. The clinical need for a safe and effective inhibitor of FGFR3 is unmet, leaving achondroplasia currently incurable. Here, we evaluated RBM-007, an RNA aptamer previously developed to neutralize the FGFR3 ligand FGF2, for its activity against FGFR3. In cultured rat chondrocytes or mouse embryonal tibia organ culture, RBM-007 rescued the proliferation arrest, degradation of cartilaginous extracellular matrix, premature senescence, and impaired hypertrophic differentiation induced by FGFR3 signaling. In cartilage xenografts derived from induced pluripotent stem cells from individuals with achondroplasia, RBM-007 rescued impaired chondrocyte differentiation and maturation. When delivered by subcutaneous injection, RBM-007 restored defective skeletal growth in a mouse model of achondroplasia. We thus demonstrate a ligand-trap concept of targeting the cartilage FGFR3 and delineate a potential therapeutic approach for achondroplasia and other FGFR3-related skeletal dysplasias.

INTRODUCTION

Achondroplasia (ACH) is the most common dwarfism in humans, occurring in between 1:15,000 and 1:40,000 live births (1). ACH is caused by mutations in the FGFR3 gene, which encodes a transmembrane receptor tyrosine kinase. Fibroblast growth factor receptor 3 (FGFR3) transduces the communication signals delivered by fibroblast growth factors (FGFs) (2). In addition to ACH, activating mutations in FGFR3 cause hypochondroplasia, SADDAN (severe achondroplasia with developmental delay and acanthosis nigricans), and lethal thanatophoric dysplasia. These conditions are collectively termed FGFR3-related skeletal dysplasias. In addition, many cases of idiopathic short stature may also be associated with mutations in FGFR3, identifying FGFR3 as a major cause of genetic dwarfism in humans (3).

In ACH, most patients carry the p.G380R substitution in the transmembrane domain of FGFR3 that activates FGFR3 signaling by increasing dimerization and phosphorylation of mutant FGFR3 dimers (4). Aberrant activation of FGFR3 alters several signaling systems necessary for proper chondrocyte proliferation and differentiation such as wingless-related integration site (WNT) pathway, cytokine/signal transducer and activator of transcription (STAT) signaling, and bone morphogenetic protein (BMP) and Hedgehog signaling (5–7). The complex molecular phenotypes induced by FGFR3 affect chondrocyte behavior, inducing proliferation arrest, degradation of cartilaginous extracellular matrix, and premature senescence. Collectively, these changes lead to disruption of the growth plate cartilage and defective endochondral ossification (8). No therapy exists for ACH except for growth hormone, which is approved for ACH in Japan and shows limited effect (9). Several experimental approaches for targeting FGFR3 are

being tested, including small chemical inhibitors of FGFR3 catalytic activity or biomolecules targeting downstream pathways of FGFR3 signaling (10). The clinical implementation of these inhibitors in ACH is complicated because the disease affects skeletal growth rather than development and, therefore, defects accumulate gradually during a growth period lasting 12 to 14 years. Because of this gradual effect, the prospective FGFR3 inhibitor must remain active during the entire period of the treatment. Toxicity of the FGFR3 therapy is unlikely to be tolerated in ACH, complicating application of chemical FGFR inhibitors (11). Alternative approaches must therefore be developed to target FGFR3 and its signaling, either alone or in combination with drugs currently in clinical evaluation for ACH.

When overexpressed in vitro, the FGFR3-G380R has a higher propensity for ligand-independent activation compared to wild-type FGFR3 (4). However, the FGFR3 is produced in low quantities in chondrocytes in vivo and thus the FGF ligand is necessary to activate both wild-type and FGFR3-G380R or their heterodimers existing in chondrocytes (12). Neutralization of FGF may therefore be a viable option to treat ACH. An RNA aptamer RBM-007, designed to neutralize the cognate FGFR3 ligand, FGF2, was recently developed. RBM-007 is composed of 36 nucleotides and binds stably and specifically to FGF2 but not to the other FGFs (13, 14). The Kd (dissociation constant) values of RBM-007 for FGF2s from human, rat, and mouse ranged between 2 and 7 pM, indicating high-affinity binding. RBM-007 blocked FGF2 interaction with FGFR1 to FGFR4, preventing signaling. FGF2 is known to induce angiogenesis and fibrosis (15). Accordingly, RBM-007 inhibited FGF2-induced angiogenesis in mice and laser-induced choroidal neovascularization and fibrosis in mice and rat models (14). On the basis of these and other preclinical studies, we have initiated a clinical study of RBM-007 to provide a therapy for exudative age-related macular degeneration, which remains as an unmet medical need (completed phase 1/2a, ongoing phase 2). In this article, we demonstrate the effect of RBM-007 in experimental in vitro and in vivo models to pathological FGFR3 signaling in ACH and identify RBM-007 as a therapeutic approach for FGFR3-related skeletal dysplasias.

RESULTS

RBM-007 inhibits FGFR3 activation by FGF2

FGFR3 is a physiological negative regulator of postnatal growth. Deletion of Fgfr3 results in overall skeletal overgrowth in mice, whereas putative loss-of-function mutations in FGFR3 cause tall stature (>97th percentile) in humans with camptodactyly, tall stature, and hearing loss (CATSHL) syndrome (16, 17). The opposite situation can be found in ACH, which is caused by gain-of-function mutations in FGFR3, and manifests as a severe dwarfism. We compared the catalytic activity of the two known CATSHL mutants, R621H and T546K, with wild-type FGFR3 and found that CATSHL mutations lead to 100% inactive FGFR3 when expressed in cultured cells (Fig. 1A and fig. S1A). A similar comparison of FGFR3 bearing the most common ACH substitution, G380R, demonstrates that G380R is only mildly activating, enhancing basal as well as FGF2-induced FGFR3 activity by 43 to 44% and 17 to 60%, depending on the cell model used (Fig. 1B and fig. S1B).

A comparison of CATSHL and ACH growth curves with FGFR3 activity allows determination of the full extent of the negative effect of FGFR3 on skeletal growth. In

Fig. 1C, we plotted the growth curves of individuals with CATSHL (n = 8 and 10 for women and men, respectively) and ACH (n = 28 and 48 for women and men, respectively) against a general population. In ACH, the inhibition of relative growth rate was 23.2% for men [95% confidence interval (CI), 15.4 to 31%] and 18% for women (11.1 to 24.9%) (Fig. 1D). The profound dwarfism that characterizes ACH is therefore the result of a long-term cumulative effect of relatively minor inhibition of growth rate. Similarly, the skeletal overgrowth seen in CATSHL stems from a minor but persistent elevation of growth rate (9.3% for men, 95% CI, 1.5 to 17%; 7.5% for women, 1 to 14.5%) (Fig. 1, C and D). Our observations suggest that therapeutically targeting ACH would require a relatively small inhibition of FGFR3 activity. We calculated that suppressing as little as 20 to 30% of FGFR3-G380R activity would produce a corresponding 20 to 30% increase of stature height in ACH (Fig. 1C, arrows).

To test whether RBM-007 inhibits the ligand-mediated activation of FGFR3, we treated cultured MCF7 or 293T cells transiently expressing FGFR3-G380R with FGF2 and determined the effect of RBM-007 on FGFR3 activation. FGFR3 autophosphorylation mediated by FGF2 was inhibited by RBM-007; a scrambled aptamer showed no effect (Fig. 1E and fig. S1C). Next, rat chondrosarcoma (RCS) chondrocytes were used to evaluate whether RBM-007 is capable of inhibiting activation of FGFR3 bearing the G380R mutation. We inactivated Fgfr1, Fgfr2, Fgfr3, and Fgfr4 loci using CRISPR-Cas9 to produce RCS cells devoid of endogenous FGFR expression. These Fgfr1 to Fgfr4 null cells were stably transfected with human FGFR3-G380R to generate RCS^ACH cells. In RCS^ACH cells, the phosphorylation of both the fibroblast growth factor receptor substrate 2 (FRS2) and ERK MAP kinase was used as surrogates for the FGFR3-G380R activation (Fig. 1F). FGF2-mediated induction of FRS2 and ERK phosphorylation in RCS^ACH cells was suppressed by RBM-007, whereas a scrambled aptamer showed no effect (Fig. 1F).

RBM-007 inhibits FGFR3 signaling in cultured chondrocytes

We next evaluated the effect of RBM-007 on cell behavior in wild-type RCS chondrocytes. RCS cells maintain a chondrocyte phenotype in culture, manifested as abundant production of extracellular matrix composed of sulfated proteoglycans and collagen type 2 (18). These cells express endogenous FGFR3 and are frequently used to model the effects of FGFR signaling in a chondrocyte cell environment (19–21).

Activation of endogenous FGFR3 by treatment with FGF2 led to potent inhibition of RCS proliferation, manifested as a growth arrest of the entire cell population in 96 hours (Fig. 2A). This phenotype was reversed by RBM-007, with nearly complete rescue achieved at ~4 times molar excess of RBM-007 over FGF2; 60 to 80% rescue was achieved with ~1.4:1 RBM-007 to FGF2 molar ratio (1.5 to 2 nM RBM-007 versus 1.2 nM FGF2) (Fig. 2B, red line). No rescue of the growth arrest was found in cells treated with scrambled aptamer.

Treatment with FGF2 caused loss of RCS cartilaginous extracellular matrix, as manifested by lack of Alcian blue staining of sulfated proteoglycans in RCS cultures. This effect was rescued by RBM-007, but not by a scrambled aptamer (Fig. 2C). The expression of collagen type 2 was lost in cells treated with FGF2; this phenotype was also restored by RBM-007 (Fig. 2E and fig. S2A). FGF2-mediated loss of extracellular matrix in RCS chondrocytes was accompanied by increased adhesion, evidenced by detection of

focal adhesions by vinculin immunocytochemistry (Fig. 2D). Increased cell spreading was also detected in FGF2-treated cells, evidenced by increased phalloidin staining indicating formation of F-actin stress fibers; the effects of FGF2 on cell spreading and adhesion were rescued by RBM-007 (Fig. 2D).

Next, we analyzed RCS chondrocytes for markers of premature senescence. As previously described, treatment with FGF2 induced senescence, manifested by up-regulation of lamin A/C and caveolin expression and down-regulation of ID2 (19). The senescence phenotype was fully reversed by RBM-007, whereas a scrambled aptamer showed no effect (Fig. 2E and fig. S2A).

To gain more insight into the mechanism of RBM-007 action, we determined its effect on downstream components of FGFR3 signaling.

In RCS cells, treatment with FGF2 triggered tyrosine phosphorylation of FRS2 and activation of mitogen-activated protein kinase kinase (MEK) and extracellular signal–regulated kinase (ERK) kinases belonging to the rat sarcoma (RAS)-ERK signaling pathway responsible for FGF-mediated growth arrest (Fig. 2F and fig. S2B) (22). The coreceptor for WNT-family morphogens, low-density lipoprotein receptor–related protein 6 (LRP6), was also phosphorylated in cells treated with FGF2, as a result of ERK pathway activation (23). FGF2-mediated activation of FGFR3 signaling was completely rescued by RBM-007, demonstrating that RBM-007 suppresses FGFR3 effects on chondrocytes by inhibition of its downstream signaling.

RBM-007 restores impaired chondrocyte differentiation in tibia organ culture

During their life cycle in vivo, chondrocytes progress through a series of cellular phenotypes involving proliferation and gradual maturation in early and late hypertrophy stages. This hypertrophic differentiation culminates in production of mineralized matrix and apoptosis followed by cartilage replacement by invading bone (24). Hypertrophic chondrocyte differentiation is impaired in ACH, resulting in a reduction in size and disorganization of the cellular architecture of the hypertrophic zone of growth plate cartilage (12).

The deleterious effect of FGFR3 activation on chondrocyte differentiation may be modeled ex vivo in mouse embryonal tibia organ culture (25). Here, we used tibia organ culture to evaluate the effect of RBM-007 on chondrocyte hypertrophic differentiation. Tibias were isolated from E18 mouse embryos and grown for 8 days in culture. Treatment with FGF2 reduced tibia growth by about 63% (Fig. 3, A and B), accompanied by reduction of hypertrophic cartilage, evidenced by loss of expression of hypertrophic chondrocyte marker Col10a1 (Fig. 3C). RBM-007 rescued the FGF2 effect on tibia growth, including restoration of Col10a1 expression (Fig. 3, A to C); no effect was found for a scrambled aptamer.

RBM-007 restores impaired differentiation of ACH chondrocytes in vitro and in vivo

Recently, we developed cartilage xenografts, consisting of proliferating chondrocytes derived from human induced pluripotent stem cells (hiPSCs) implanted subcutaneously into SCID mice. These xenografts form morphologically correct growth plate cartilage in

vivo (26). When compared to wild-type hiPSCs, hiPSCs derived from individuals with ACH fail to produce cartilage in vitro and form abnormal growth plates in in vivo xenografts (27). We wondered whether RBM-007 would rescue defective chondrocyte differentiation in ACH xenografts.

hiPSCs were derived from three pediatric patients with ACH (fig. S3) and subjected to chondrocytic differentiation (Fig. 4A). After 8 weeks, ACH hiPSCs treated with RBM-007 formed spherical structures of 2 to 5 mm in diameter, containing small and round chondrocytes surrounded by abundant cartilaginous matrix as shown by Safranin O staining for sulfated proteoglycans and quantitative reverse transcription polymerase chain reaction (qRT-PCR) analysis for expression of mature cartilage markers SOX9, COL2A1, and ACAN (Fig. 4, B and C). In contrast, only poorly differentiated, immature cartilage was formed in cultures treated with vehicle.

After in vitro chondrocytic differentiation, the hiPSC-derived cartilage was implanted subcutaneously in C.B-17/lcr-scid/scidJcl mice and grown for an additional 6 weeks (Fig. 4A). Four different conditions were evaluated for wild-type and ACH xenografts: Exposure to RBM-007 during either in vitro or in vivo growth, both, or neither (Fig. 4D). Histological analysis revealed formation of mature chondrocytes in ACH xenografts treated with an (in vitro/in vivo) RBM-007/vehicle or RBM-007/RBM-007 protocol, but not in xenografts treated with vehicle/vehicle or vehicle/RBM-007 (Fig. 4E). These data demonstrate that the inhibitory effect of RBM-007 on FGFR3 signaling during chondrocytic differentiation in vitro allows for maintenance of mature ACH cartilage in vivo.

Pathological activation of FGFR3 leads to suppression of chondrocyte hypertrophy in mouse or human growth plate, manifested as disappearance of enlarged chondrocytes above the chondro-osseous junction (11). We therefore used chondrocyte diameter as a surrogate for hypertrophic differentiation. Figure 4F shows a significant ($P < 0.001$) increase of chondrocyte diameter of ACH xenografts treated with the RBM-007/RBM-007 protocol compared to xenografts treated with RBM-007/vehicle. These data demonstrate restoration of hypertrophic chondrocyte differentiation by RBM-007 in vivo. In wild-type hiPSCs, RBM-007 did not affect chondrogenic differentiation in vitro, and xenografts derived from wild-type hiPSCs acquired a similar degree of in vivo hypertrophic differentiation regardless of RBM-007 treatment (Fig. 4F).

RBM-007 partially rescues skeletal growth defects in an FGF2-overexpressing mouse model

Next, we used a mouse model overexpressing human FGF2 to evaluate an RBM-007 effect on bone growth. FGF2-overexpressing (FGF2) mice were developed according to a previously published model (28). Compared to their wild-type littermates, the FGF2 mice were smaller, with a shorter body and limbs and a short snout (Fig. 5A).

All four existing protein variants of FGF2, generated by alternative translation of the FGF2 transcript (29), were found expressed in the FGF2 mice. Both 18-kDa low–molecular weight FGF2 and its high–molecular weight variants (22, 22.5, and 24 kDa) were significantly elevated in kidney ($P < 0.001$), liver ($P < 0.001$), brain ($P < 0.001$), and femurs ($P < 0.01$) harvested from FGF2 mice compared to expression of endogenous FGF2 in wild-type littermates (Fig. 5B).

We evaluated two protocols of RBM-007 administration during the P3 to P24 growth period, consisting of subcutaneous injections of RBM-007 (1 mg/kg) every 2 days (2D) or 4 days (4D) (Fig. 5C). Body weight and length were measured at P3, P10, P17, and P24. No increase in body weight or length was found in control animals treated with RBM-007 compared to the vehicle. Similarly, weight and overall body length were unaffected by RBM-007 in FGF2 animals except for animals treated with the 4D protocol, where the body weight weakly increased at P24 (Fig. 5D and fig. S4). The lack of a substantial RBM-007 effect on the weight and body length of FGF2 mice may be attributed to the high expression of the transgenic FGF2 (Fig. 5B), which was not completely neutralized at the RBM-007 dose used (1 mg/kg). Because FGFR3 signaling affects predominantly the length of the extremities but not the trunk, and unlike the legs in humans, the hindlimbs do not contribute to the overall body length in rodents, we determined the sizes of femurs and tibias in animals treated with RBM-007. No effect on femur or tibia length was found in wild-type animals at the end of the treatment period (P24). In contrast, the FGF2 mice responded to RBM-007 administered according to the 2D or 4D protocol with moderate but statistically significant elongation of both tibia ($P < 0.001$ for both protocols) and femurs ($P < 0.01$ for the 2D protocol; $P < 0.001$ for the 4D protocol) (Fig. 5E).

RBM-007 rescues skeletal defects in ACH mice

FGF2 is expressed in rat and human growth plate cartilage (30, 31), but there is no evidence of its expression in mouse. Western blot analysis of endogenous FGF2 expression in growth plates harvested from femurs of wild-type P7 mice detected all four existing protein variants of FGF2 (18, 22, 22.5, and 24 kDa), which were expressed in wild-type growth plates (Fig. 6, A and B). Next, we determined FGF2 protein expression in the Fgfr3^ACH mice (ACH mice). These These animals express murine FGFR3 with an ACH mutation (G380R) in chondrocytes under the control of the Col2a1 promoter/enhancer and show typical skeletal features of humans with ACH, such as impaired growth of long bones and a short snout, modeling the midface hypoplasia observed in humans (32). Growth plates harvested from ACH mice also expressed FGF2, but no significant difference was found in the quantity of total FGF2 or its isoforms between wild-type and ACH growth plates (Fig. 6B; $P > 0.05$). To localize FGF2 in the growth plate with more precision, sections of wild-type and ACH growth plates were stained by Picrosirius red with or without FGF2 antibody. FGF2 was expressed throughout the growth plate, showing signal in reserve, proliferating, hypertrophic zones, perichondrium, and perivascular region. No differences in FGF2 localization were found between wild-type and ACH mice (Fig. 6C).

We next administered RBM-007 to ACH mice by subcutaneous injection for 18 days (P3 to P21, 2-day injection interval) at a dose of 10 mg/kg (Fig. 7A). ACH mice treated with RBM-007 showed increased body size and snout elongation compared to vehicle-treated animals (Fig. 7B). This was confirmed by analyses of body length and weight, which showed statistically significant increases in both parameters in RBM-007–treated ACH mice (starting at P13 with $P < 0.01$) (Fig. 7C). Similarly, the measurements of femur and tibia length at the end of the treatment period (P21) demonstrated significant ($P < 0.001$) elongation in RBM-007–treated ACH mice, compared to vehicle-treated animals; no RBM-007 effect was found in wild-type animals (Fig. 7D).

Overall femur morphology in ACH mice treated with RBM-007 or vehicle for 18 days was visualized by x-ray tomography. RBM-007 rescued growth retardation in ACH femurs; no effect of RBM-007 was found in wild-type femurs (Fig. 8A). Wall thickness analyses, generated by micro–computed tomography (μCT) imaging, demonstrated an increase of bone thickness in the diaphysis of ACH femurs treated by RBM-007 to a degree comparable with wild-type femurs (Fig. 8B). Histological analyses demonstrated adipocyte expansion and reduced spongy bone and primary lamellae in the osteoid zone of ACH femurs (Fig. 8C), together with suppression of prehypertrophic and hypertrophic zones of the growth plate cartilage (Fig. 8D). This abnormal bone and cartilage morphology was corrected by RBM-007.

DISCUSSION

It is estimated that approximately 280,000 children live with ACH worldwide (1, 33, 34). A prospective treatment would need to be administered during the entire postnatal growth period (up to 14 years) and, if started early, could potentially normalize skeletal development, correcting most of the pathological features of ACH. The major domain of FGFR3 expression is growth plate cartilage, with minor expression found in intestinal crypts, skin, and bone (35–37). It is thus expected that if specific, FGFR3 targeting would produce few side effects, an important factor for a long-term therapy in children. Moreover, FGFR3 is a physiological negative regulator of growth, as evidenced by skeletal overgrowth in mice with deleted Fgfr3 or tall stature in humans carrying loss-of-function mutations in FGFR3 (16, 17). Thus, we speculate that an effective FGFR3 inhibitor could potentially be repurposed for other skeletal dysplasias caused by defective chondrocyte proliferation, including idiopathic short statures.

In this study, we demonstrate an approach to target FGFR3 signaling in skeletal dysplasia based on a ligand-trap concept. We show that neutralization of FGF2 ligand by RNA aptamer RBM-007 restores defective bone growth in FGFR3-related skeletal dysplasia in mice. RBM-007 has two advantages when compared to other approaches currently in development for ACH. First, RBM-007 is already undergoing a clinical evaluation in the United States (NCT03633084 and NCT04200248), and a clinical trial program for ACH treatment was initiated in Japan in July 2020, during revisions of this study (JapicCTI-205345). Second, RBM-007 acts as a direct inhibitor of FGFR3, targeting FGFR3 signaling pathway at the level of FGFR3 activation. The RBM-007–mediated rescue of the growth defect in femurs and tibias in ACH mice was comparable with previous experimental approaches to target FGFR3, including treatment with rosuvastatin (27), parathyroid hormone (38), soluble FGFR3 (39), meclozine (40), and small chemical FGFR3 inhibitor BGJ398 (41). Among candidate drugs developed for ACH, vosoritide is currently in the third phase of clinical trials for ACH (10) and, thus, has an advantage in application compared to RBM-007. Vosoritide is a stable analog of C-natriuretic peptide (CNP) (42), which exploits the natural mechanism regulating definitive stature height in humans, where the CNP pathway increases skeletal growth via mechanistic inhibition of the FGFR3 pathway (43).

Vosoritide inhibits FGFR3 signaling indirectly, via activation of an opposing signaling pathway. Because signaling pathways are usually negatively or positively modulated at many levels, the outcomes of long-term vosoritide therapy may depend on these regulations. Although this is a poorly characterized area of cartilage biology, several of these regulations are already known, for instance, phosphodiesterases, which limit

vosoritide signaling via cGMP degradation, or FGFR3-mediated inactivation of CNP receptor NPRB via dephosphorylation (44, 45). In addition, circulating CNP is elevated in individuals with ACH (46), and the zone of NPRB expression in growth plate cartilage is markedly expanded in ACH mice (47), both suggesting resistance of aberrant FGFR3 signaling to CNP.

In conclusion, the vosoritide trial demonstrates increased relative growth velocity in ACH patients (10). It is not yet clear whether the robust initial response to vosoritide will later diminish, owing to resistance mechanisms typical for natriuretic peptides (48, 49) and other factors that may limit the overall clinical effect. Therapies conceptually different from vosoritide should therefore be investigated and developed. Direct inhibitors of FGFR3, such as RBM-007 described here, could also potentially be used either alone or in combination with vosoritide for full restoration of skeletal growth in patients with skeletal dysplasia, although this remains to be tested in future studies.

RBM-007 inhibited activation of FGFR3 signaling in cultured chondrocytes in vitro as well as in tibia organ cultures and cartilage xenografts differentiated from hiPSCs derived from individuals with ACH. More importantly, when administered to mice, RBM-007 restored defective skeletal growth in the ACH model. The current study analyzed the effect of RBM-007 on the skeleton of ACH mice by determining the overall femur morphology by μCT imaging and histological analyses of femoral growth plates. Analyses of the RBM-007 effect on the axial skeleton, such as intervertebral discs, chest, and craniofacial bones, were not carried out here and will be addressed in a follow-up study. The efficacy of RBM-007 in ACH is currently unknown and needs to be evaluated in human studies. The clinical trial program for RBM-007 in ACH treatment was initiated in July 2020 (JapicCTI-205345).

Our data suggest that FGF2 is a physiological cognate ligand for FGFR3 in the growth plate cartilage. Other FGF ligands may activate FGFR3 in experimental cell models, including FGF1, FGF8, FGF9, FGF17, FGF18, and FGF20 (50). Activation of FGFR3 by alternative FGFs will be insensitive to RBM-007 inhibition and thus may represent a limitation to RBM-007 use in ACH therapy. In mice, deletion of Fgf18 leads to increased chondrocyte proliferation and differentiation (51), similar to that observed in Fgfr3-null mice (16). In addition, deletion of Fgf9 also leads to limb shortening in mice (52), implying that FGF9 and FGF18 act as FGFR3 ligands in mice. FGF9 and FGF18 are not expressed in growth plate cartilage but in adjacent tissues such as the mesenchyme surrounding the cartilage condensations in early limb development, or in perichondrium in later stages, implying that the perichondrium regulates FGFR3 activity in murine growth plate via FGF9 and FGF18 secretion. It is unclear to what extent the perichondrium-based FGF ligands regulate FGFR3 during the entire period of postnatal growth, which is the main process affected by aberrant FGFR3 signaling in ACH.

In humans, the overall size of the growing long bones makes the perichondrial FGFs unlikely to efficiently penetrate into the entire growth plate cartilage. FGF9 and FGF18 are not expressed in human perichondrium or in the growth plate cartilage (31). In addition, loss-of-function mutations in FGF9 cause multiple synostoses syndrome, manifested by fusions of proximal interphalangeal, carpal-tarsal, and humeroradial joints (53). The stature is normal in patients with multiple synostoses syndrome and not elevated as observed in patients with CATSHL with FGFR3 loss-of-function mutations (17). This

demonstrates that FGF9 loss does not phenocopy the FGFR3 inactivation in humans, making FGF9 an unlikely physiological ligand for FGFR3 in the growth plate.

Together, the evidence suggests that other FGFs are involved in FGFR3 activation in humans, such as FGF2, which is abundantly expressed in the human growth plate (31). In the present study, we report that FGF2 is also expressed in mouse growth plate cartilage and that its neutralization by RBM-007 restores the defective growth in the mouse model of ACH.

MATERIALS AND METHODS

Study design

The aim of this study was to assess the effect of RBM-007 on FGFR3 signaling and chondrocyte and bone development using cultured chondrocytes, human cartilage organoid cultures, and mouse tibia organ cultures. In addition, two mouse models of skeletal dysplasia were used to evaluate the efficacy of RBM-007. We designed curative effect studies in human FGF2-overexpressing mice and ACH mice to examine the effect of RBM-007 on bone growth.

Cell, organoid, and organ culture experiments were conducted in at least three independent replicates and consisted of technical replicates if relevant for proper analysis. Investigators were not blinded. No data were excluded from analyses. For in vivo studies, sex- and age-matched animals were randomly assigned to each group. The number of animals in each study was determined by investigators based on pilot studies and previous experience with disease models. Control and treatment groups, sample sizes, amounts of independent experiments, and statistical tests used are specified in figures or their legends.

FGF2 and ACH animal experiments were conducted under protocols approved by the Animal Ethical Committee at TransGenic Inc. Institute of Cancer Research (ICR) mouse experiments were according to the Central Commission for Animal Welfare of the Ministry of Agriculture of the Czech Republic (§16a, law no. 246/1992 Sb.) and regulations approved by the Laboratory Animal Science Committee of the Institute of Animal Physiology and Genetics. Cartilage xenograft animal experiments were approved by the institutional review board, animal committee, and biosafety committee of Osaka University.

Analysis of experimental data was not blinded. Primary data are reported in data file S1.

Cell culture, preparation of cell and tissue extracts, Western blot, and quantitative PCR

RCS, 293T, and MCF7 cells were propagated in Dulbecco's modified Eagle's medium (DMEM) supplemented with 10% fetal bovine serum (FBS) and antibiotics (Invitrogen). Cells were transfected using FuGENE6 (Promega). Vectors expressing V5-tagged hFGFR3 were described previously (54). R621H and T546K mutations were introduced into FGFR3 by site-directed mutagenesis (Agilent). Cell proliferation was determined by crystal violet staining (25). FGF2 was obtained from R&D Systems.

For Western blots, cells were lysed in sample buffer [125 mM Tris-HCl (pH 6.8), 20% glycerol, 4% SDS, 5% β-mercaptoethanol, and 0.02% bromophenol blue]. Mouse tissue samples were extracted into lysis buffer [50 mM Tris-HCl (pH 7.4), 150 mM NaCl, 0.5% NP40, 1 mM EDTA, protease inhibitor, and 1 mM orthovanadate], cleared by centrifugation, and concentrations were equalized using Bio-Rad protein assay. Femurs were dissected from at least three males and three females at P7; cartilage protein was extracted in radioimmunoprecipitation assay (RIPA) buffer with proteinase and phosphatase inhibitors. Lysates were resolved by SDS–polyacrylamide gel electrophoresis, transferred onto PVDF membrane, and visualized by chemiluminescence (Thermo Fisher Scientific).

The antibodies used were as follows: V5 (Invitrogen); pLRP6^T1572 (Millipore); collagen 2 (Cedarlane); FGF2 and FRS2 (Sigma-Aldrich); MEK1, FRS2, and actin (Santa Cruz Biotechnology); and phosphorylated FGFR (pFGFR)^Y653/Y654, ERK, pERK^T202/Y204, LRP6, pMEK1/2^Ser217/221, pFRS2^Y436, caveolin, lamin A/C, ID2, α-tubulin, and vinculin (Cell Signaling Technology). Signal quantification was performed using ImageJ (https://imagej.nih.gov/ij/).

Total RNA was isolated using NucleoSpin RNA (Takara Bio), with 200 ng of total RNA used as a template for cDNA synthesis using the ReverTra Ace system (Toyobo). Quantitative PCR (qPCR) was performed on a QuantStudio 7 Flex PCR system (Applied Biosystems) using Thunderbird SYBR qPCR Mix (Toyobo). Primer sequences are provided in table S1.

Generation of RCS^ACH cells

CRISPR-Cas9 was used to knock out Fgfr1 to Fgfr4 in RCS cells, using a pair of Cas9 nickases for each gene. Successful disruption was confirmed by Sanger sequencing. Table S2 shows target sequences and primers used for amplification of genomic sequences. The piggyBac transposase system was used for stable integration of human C-terminally V5-tagged FGFR3-G380R into Fgfr1–Fgfr4 null RCS cells. TR01F plasmid was used as the backbone of the integration cassette (55), in which a nuclear factor κB (NF-κB)–responsive element and a Luc2 gene were replaced by an attenuated CMV promoter and the FGFR3-G380R sequence.

Growth curve modeling

Data used to generate growth charts were obtained from previous publications for non-ACH and non-CATSHL (unaffected) individuals (56), or from individuals with ACH (n = 2 women and n = 48 men) (57) or CATSHL (n = 8 women and n = 10 men) (17, 58, 59). Published ACH data were supplemented by data obtained from the ReACH Registry (www.achondroplasia-registry.cz). CATSHL growth curves were based on the unaffected population, assuming that average height for those with CATSHL was above or equal to the 97th percentile of the normal population (17). Confidence intervals (CIs) for growth curves of unaffected individuals were based on the mean and standard deviation (SD) of the normal population. CIs for CATSHL were based on the 97th percentile of the unaffected population as estimated from its mean and SD. Mean and SD for growth curves for individuals with ACH were obtained from (57). The PROC TRANSREG procedure in SAS 9.4 (SAS Institute) was used for smoothing of growth curves. To compute growth

velocity (in centimeters per month), PROC ANOVA was used to compare mean values of growth velocity calculated over the timeline.

Tibia organ culture and Col10a1 RNAScope

Tibias from E18 mouse embryos (ICR line, Masaryk University) were placed on Millipore filters above a metal mesh and cultured in F12/DMEM supplemented with 10% FBS, ascorbic acid (50 μg/ml), and 10 mM β-glycerol phosphate for 8 days. Media supplemented with FGF2 (100 ng/ml), RBM-007 (100 nM), or scrambled aptamer (100 nM) were changed daily. Tibia length was measured at day 0 and at the end of cultivation (day 8) using Axio Vision (Zeiss). For histology, tibias were fixed in 4% paraformaldehyde (PFA), decalcified in 10% EDTA, dehydrated in an ethanol series, embedded in paraffin, and stained with hematoxylin and eosin. Col10a1 expression was detected using the Mm-Col10a1 probe with RNAScope Technology (ACD Bio). The hybridized probe was visualized using the TSA-Plus Cyanine 3 system (Perkin-Elmer). Nuclei were stained with 4′,6-diamidino-2-phenylindole (DAPI).

hiPSC-derived cartilage and xenograft transplantation

The hiPSC line 409B2 (healthy control) and three hiPSC lines derived from pediatric patients with ACH (ACH1 to ACH3) were gifts from N. Tsumaki, Center for iPS Cell Research and Application, Kyoto University, Kyoto, Japan. hiPSCs were generated as described previously (60). For mesenchymal stem cell (MSC) differentiation (61), iPSCs were allowed to form embryoid bodies (EBs) in hiPSC medium supplemented with BMP4 (10 ng/ml; PeproTech). EB cells were spread in type IV collagen–coated dishes (Nippi) and grown in αMEM (Thermo Fisher Scientific) containing 10% FBS, basic FGF (bFGF; 5 ng/ml), 0.1 mM 2-mercaptoethanol, BMP4 (10 ng/ml), activin A (3 ng/ml), 5 mM LiCl, and 0.5% penicillin-streptomycin. Media were changed on days 2 and 4.

On day 6, differentiated cells were reacted with CD140a-APC (BioLegend) and VEGFR2/KDR-PE antibody (R&D Systems). Proximal side population cells were purified by flow cytometry (FACSAria II, BD Biosciences) and resuspended in type IV collagen–coated dishes in αMEM (10% FBS and 0.1 mM β-mercaptoethanol). For osteocyte differentiation, MSCs derived from hiPSCs were grown in DMEM supplemented with 10% FBS and 10 mM β-glycerophosphate, 100 nM dexamethasone, 50 μM ascorbic acid, and BMP4 (10 ng/ml). For adipocyte differentiation, MSCs were grown in DMEM containing 10% FBS, 1 μM dexamethasone, insulin (5 μg/ml), 500 μM 3-isobutyl-1-methylxanthine, and 50 μM indomethacin. Cells were harvested on day 28 for analysis.

hiPSCs were differentiated to produce hiPSC-derived cartilage over 8 weeks as previously described (62). Briefly, hiPSCs were maintained in Essential 8 medium [penicillin (50 U/ml) and streptomycin (50 mg/ml)] in Matrigel-coated dishes. hiPSCs formed high-density colonies of 1 × 10^5 to 2 × 10^5 cells after 2–3 weeks in feeder-free culture.

Differentiation into mesendodermal cells was performed in DMEM/F12 containing WNT3A (10 ng/ml), activin A (10 ng/ml), 1% ITS, 1% FBS, penicillin (50 U/ml), and streptomycin (50 mg/ml). On day 3, medium was changed to DMEM with 1% ITS, 1% FBS, 2 mM L-glutamine, 10^–4 M non-essential amino acids, 1 mM sodium pyruvate,

ascorbic acid (50 μg/ml), BMP2 (10 ng/ml), TGFβ1 (10 ng/ml), and GDF5 (10 ng/ml) to commit cells to the chondrocytic lineage. FGF2 (10 ng/ml; WAKO) was added from day 3 to day 14.

Multi-layered nodules formed by day 14, physically separated from the dish bottom to form particles, and were transferred to low-attachment surface plates (Corning). On day 56, hiPSC-derived cartilaginous particles were transplanted subcutaneously into the backs of 4-week-old male CB-17/Icr-scid/scidJcl (SCID) mice (CLEA Japan). Mice were euthanized 6 weeks after transplantation, and bone structures of the grafts were confirmed by μCT imaging (R-μCT, Rigaku). Surgical transplantation, x-ray imaging, and euthanasia were performed under anesthesia.

For treatment of the cartilage xenograft model with RBM-007, mice were divided into groups of six (three treated with RBM-007, 10 mg/kg, and three treated with PBS). One day after transplantation, RBM-007 was injected subcutaneously into the caudal portion, distant from the xeno-graft location (upper back), and administered twice per week for 6 weeks. Mice were euthanized 6 weeks after transplantation, and grafts were recovered for histological analysis.

Human FGF2-overexpressing mice and ACH mice

The FGF2-overexpressing mice were generated as previously described (28). Briefly, a PGK promoter–human FGF2–PGK polyA expression vector was digested, and the transgene containing the PGK promoter, human FGF2, and PGK polyA was isolated and injected into the pronucleus of fertilized eggs from C57BL/6N wild-type female mice. The eggs were then transferred to recipient ICR female mice to generate F0 mice. Genotyping of transgenic mice was performed using the primer set PGK-pro F (TACCGGGTAGGGGAGGCGCTTTTCCC) and PGK-polyA_R (TCTATAGATCATGAGTGGGAGGAATGAGC). F0 founder males carrying the transgene were crossed with C57BL/6N females to establish the transgenic mouse line. One line exhibiting ACH-like phenotypes was selected for further study. To produce sufficient FGF2 transgenic hemizygous mice, sperm from F1 hemizygous males was used for in vitro fertilization with eggs from C57BL/6N wild-type females. Embryos were transferred to recipient ICR females, and pups were weaned. Starting 3 days after birth, RBM-007 was administered subcutaneously every 2 or 4 days at a dose of 1 mg/kg until day 24. Genotypes were confirmed on day 13. Body weight and nose-to-anus length were measured from day 3 to day 24, and femur and tibia lengths were measured with a digital caliper to 0.1 mm on day 24; the average of right and left limbs was recorded for each animal.

Fgfr3^ACH^ mice (ACH mice) express murine FGFR3 with the ACH mutation (p.G380R) specifically in chondrocytes under the Col2a1 promoter/enhancer (32). Sperm from hemizygous Fgfr3^ACH^ males, provided by D. M. Ornitz (Washington University School of Medicine), was used for in vitro fertilization with eggs from C57BL/6N wild-type females. Embryos were transferred to recipient ICR females, and pups were weaned. Starting at postnatal day 3 (P3), RBM-007 (10 mg/kg) or vehicle (physiological saline) was administered subcutaneously every other day until P24. Genotypes were determined at P13 using the primer set RBM01FE_F (AGGTGGCCTTTGACACCTACCAGG) and RBM01FE_R (TCTGTTGTGTTTCCTCCCTGTTGG). Body weight and naso-anal length were measured every other day from P3 to P21, and femur and tibia lengths were

measured at P21 with a digital caliper to 0.1 mm, with the average of right and left limbs recorded per animal. All experiments were approved by the Animal Ethical Committee of TransGenic Inc. (protocols 2016J05, 2018J08, and 2018J12).

Histology and immunostaining

Crystal violet staining was carried out as described before (19). For Alcian blue staining, the cells were fixed with 4% paraformaldehyde, stained with 1% Alcian blue (Sigma-Aldrich) in 3% acetic acid, washed with water, and mounted in glycerol. The actin fibers were visualized by Phalloidin–Alexa Fluor 594 staining (Thermo Fisher Scientific). Cells were then stained with vinculin–fluorescein isothiocyanate (FITC) antibody (Sigma-Aldrich). Mice femurs were dissected and fixed in 4-PFA 4% overnight, dehydrated, and embedded in paraffin. Seven-micrometer sections were stained with Picrosirius red and hematoxylin for contrast. For immunohistochemistry, sections were treated with citrate buffer for antigen retrieval and quenched by peroxidase. FGF2 antibody (LifeSpan Biosciences) was incubated overnight 1:100. Sections were developed with the histostain plus kit with 3,3′-diaminobenzidine (DAB) as chromogen (Invitrogen). Xenografts were removed, fixed with 4% paraformaldehyde, processed, and embedded in paraffin. Semiserial sections were prepared and stained with Safranin O. For Alizarin red staining, cells were stained with 2% Alizarin red. For Oil Red O staining, cells were rinsed with 60% 2-propanol and stained with Oil Red O solution. The diameter of hypertrophic chondrocytes was measured with ImageJ.

μCT analysis

μCT scanning was performed using laboratory system GE Phoenix v|tome|x L 240 (GE Sensing & Inspection Technologies GmbH), equipped with 180 kV/15 W maximum power nanofocus x-ray tube, at the following parameters: voltage, 60 kV; current, 200 μA; exposure time, 500 ms averaging three projections. Over 360° rotation, 1500 images were taken, the voxel size of the dataset was set to 9.5 μm, and 0.2-mm aluminum foil was used to filter x-ray. GE phoenix datos|x 2.0 software was used for tomographic reconstruction. All three-dimensional (3D) visualizations and measurements were performed in VG Studio MAX 3.4 software (Volume Graphics GmbH). Sphere-based wall thickness analysis in VG studio software was used to assess thickness of the examined samples by fitting spheres inside the sample in 3D space. The thickness was defined by diameter of the fitted sphere.

Statistical analysis

All experiments were performed in at least triplicate; the actual number of independent experiments is indicated in the figures and their legends. Statistical analyses were done in GraphPad Prism using one-way analysis of variance (ANOVA) (with Bonferroni's or Dunnett's correction) or Welch's t test; the test is specified in each figure legend. The following significance levels were used: *$P < 0.05$, **$P < 0.01$, and ***$P < 0.001$; P values ≥ 0.05 were considered not significant. For growth curve modeling, the P value for Tukey's multiple comparison test and 95% CI for mean of the velocity comparison were obtained using PROC ANOVA in SAS 9.4.

REFERENCES AND NOTES

1. I. M. Orioli, E. E. Castilla, J. G. Barbosa-Neto, The birth prevalence rates for the skeletal dysplasias. J. Med. Genet. 23, 328–332 (1986).
2. N. Itoh, D. M. Ornitz, Fibroblast growth factors: From molecular evolution to roles in development, metabolism, and disease. J. Biochem. 149, 121–130 (2011).
3. S. G. Kant, I. Cervenkova, L. Balek, L. Trantirek, G. W. E. Santen, M. C. de Vries, H. A. van Duyvenvoorde, M. J. R. van der Wielen, A. J. M. H. Verkerk, A. G. Uitterlinden, S. E. Hannema, J. M. Wit, W. Oostdijk, P. Krejci, M. Losekoot, A novel variant of FGFR3 causes proportionate short stature. Eur. J. Endocrinol. 172, 763–770 (2015).
4. L. He, W. Horton, K. Hristova, Physical basis behind achondroplasia, the most common form of human dwarfism. J. Biol. Chem. 285, 30103–30114 (2010).
5. C. Li, L. Chen, T. Iwata, M. Kitagawa, X. Y. Fu, C. X. Deng, A Lys644Glu substitution in fibroblast growth factor receptor 3 (FGFR3) causes dwarfism in mice by activation of STATs and ink4 cell cycle inhibitors. Hum. Mol. Genet. 8, 35–44 (1999).
6. K. Chlebova, V. Bryja, P. Dvorak, A. Kozubik, W. R. Wilcox, P. Krejci, High molecular weight FGF2: The biology of a nuclear growth factor. Cell. Mol. Life Sci. 66, 225–235 (2009).
7. H. Qi, M. Jin, Y. Duan, X. Du, Y. Zhang, F. Ren, Y. Wang, Q. Tian, X. Wang, Q. Wang, Y. Zhu, Y. Xie, C. Liu, X. Cao, Y. Mishina, D. Chen, C. Deng, Z. Chang, L. Chen, FGFR3 induces degradation of BMP type I receptor to regulate skeletal development. Biochim. Biophys. Acta 1843, 1237–1247 (2014).
8. D. M. Ornitz, L. Legeai-Mallet, Achondroplasia: Development, pathogenesis, and therapy. Dev. Dyn. 246, 291–309 (2017).
9. T. Yorifuji, S. Higuchi, R. Kawakita, Growth hormone treatment for achondroplasia. Pediatr. Endocrinol. Rev. 16, 123–128 (2018).
10. R. Savarirayan, M. Irving, C. A. Bacino, B. Bostwick, J. Charrow, V. Cormier-Daire, K.-H. Le Quan Sang, P. Dickson, P. Harmatz, J. Phillips, N. Owen, A. Cherukuri, K. Jayaram, G. S. Jeha, K. Larimore, M.-L. Chan, A. Huntsman Labed, J. Day, J. Hoover-Fong, C-type natriuretic peptide analogue therapy in children with achondroplasia. N. Engl. J. Med. 381, 25–35 (2019).
11. I. Gudernova, I. Vesela, L. Balek, M. Buchtova, H. Dosedelova, M. Kunova, J. Pivnicka, I. Jelinkova, L. Roubalova, A. Kozubik, P. Krejci, Multikinase activity of fibroblast growth factor receptor (FGFR) inhibitors SU5402, PD173074, AZD1480, AZD4547, and BGJ398 compromises the use of small chemicals targeting FGFR catalytic activity for therapy of short-stature syndromes. Hum. Mol. Genet. 25, 9–23 (2016).
12. S. Foldynova-Trantirkova, W. R. Wilcox, P. Krejci, Sixteen years and counting: The current understanding of fibroblast growth factor receptor 3 (FGFR3) signaling in skeletal dysplasias. Hum. Mutat. 33, 29–41 (2012).
13. L. Jin, Y. Nonaka, S. Miyakawa, M. Fujiwara, Y. Nakamura, Dual therapeutic action of a neutralizing anti-FGF2 aptamer in bone disease and bone cancer pain. Mol. Ther. 24, 1974–1986 (2016).
14. Y. Matsuda, Y. Nonaka, S. Futakawa, H. Imai, K. Akita, T. Nishihata, M. Fujiwara, Y. Ali, R. B. Bhisitkul, Y. Nakamura, Antiangiogenic and antiscarring dual action of an anti-fibroblast growth factor 2 aptamer in animal models of retinal disease. Mol. Ther. Nucleic Acids 17, 819–828 (2019).
15. G. S. Schultz, M. B. Grant, Neovascular growth factors. Eye 5, 170–180 (1991).

16. J. S. Colvin, B. A. Bohne, G. W. Harding, D. G. McEwen, D. M. Ornitz, Skeletal overgrowth and deafness in mice lacking fibroblast growth factor receptor 3. Nat. Genet. 12, 390–397 (1996).
17. R. M. Toydemir, A. E. Brassington, P. Bayrak-Toydemir, P. A. Krakowiak, L. B. Jorde, F. G. Whitby, N. Longo, D. H. Viskochil, J. C. Carey, M. J. Bamshad, A novel mutation in FGFR3 causes camptodactyly, tall stature, and hearing loss (CATSHL) syndrome. Am. J. Hum. Genet. 79, 935–941 (2006).
18. K. Mukhopadhyay, V. Lefebvre, G. Zhou, S. Garofalo, J. H. Kimura, B. de Crombrugghe, Use of a new rat chondrosarcoma cell line to delineate a 119–base pair chondrocyte-specific enhancer element and to define active promoter segments in the mouse Pro-α1(II) collagen gene. J. Biol. Chem. 270, 27711–27719 (1995).
19. P. Krejci, J. Prochazkova, J. Smutny, K. Chlebova, P. Lin, A. Aklian, V. Bryja, A. Kozubik, W. R. Wilcox, FGFR3 signaling induces a reversible senescence phenotype in chondrocytes similar to oncogene-induced premature senescence. Bone 47, 102–110 (2010).
20. P. Krejci, B. Masri, V. Fontaine, P. B. Mekikian, M. Weis, H. Prats, W. R. Wilcox, Interaction of fibroblast growth factor and C-natriuretic peptide signaling in regulation of chondrocyte proliferation and extracellular matrix homeostasis. J. Cell Sci. 118, 5089–5100 (2005).
21. L. Dailey, E. Laplantine, R. Priore, C. Basilico, A network of transcriptional and signaling events is activated by FGF to induce chondrocyte growth arrest and differentiation. J. Cell Biol. 161, 1053–1066 (2003).
22. P. Krejci, V. Bryja, J. Pachernik, A. Hampl, R. Pogue, P. Mekikian, W. R. Wilcox, FGF2 inhibits proliferation and alters the cartilage-like phenotype of RCS cells. Exp. Cell Res. 297, 152–164 (2004).
23. P. Krejci, A. Aklian, M. Kaucka, E. Sevcikova, J. Prochazkova, J. K. Masek, P. Mikolka, T. Pospisilova, T. Spoustova, M. Weis, W. A. Paznekas, J. H. Wolf, J. S. Gutkind, W. R. Wilcox, A. Kozubik, E. W. Jabs, V. Bryja, L. Salazar, I. Vesela, L. Balek, Receptor tyrosine kinases activate canonical WNT/β-catenin signaling via MAP kinase/LRP6 pathway and direct β-catenin phosphorylation. PLOS ONE 7, e35826 (2012).
24. E. Kozhemyakina, A. B. Lassar, E. Zelzer, A pathway to bone: Signaling molecules and transcription factors involved in chondrocyte development and maturation. Development 142, 817–831 (2015).
25. L. Balek, I. Gudernova, I. Vesela, M. Hampl, V. Oralova, M. Kunova Bosakova, M. Varecha, P. Nemec, T. Hall, G. Abbadessa, N. Hatch, M. Buchtova, P. Krejci, ARQ 087 inhibits FGFR signaling and rescues aberrant cell proliferation and differentiation in experimental models of craniosynostoses and chondrodysplasias caused by activating mutations in FGFR1, FGFR2, and FGFR3. Bone 105, 57–66 (2017).
26. T. Kimura, T. Ozaki, K. Fujita, A. Yamashita, M. Morioka, K. Ozono, N. Tsumaki, Proposal of patient-specific growth plate cartilage xenograft model for FGFR3 chondrodysplasia. Osteoarthr. Cartil. 26, 1551–1561 (2018).
27. A. Yamashita, M. Morioka, H. Kishi, T. Kimura, Y. Yahara, M. Okada, K. Fujita, H. Sawai, S. Ikegawa, N. Tsumaki, Statin treatment rescues FGFR3 skeletal dysplasia phenotypes. Nature 513, 507–511 (2014).
28. J. D. Coffin, R. Z. Florkiewicz, J. Neumann, T. Mort-Hopkins, G. W. Dorn II, P. Lightfoot, R. German, P. N. Howles, A. Kier, B. A. O'Toole, Abnormal bone

growth and selective translational regulation in basic fibroblast growth factor (FGF-2) transgenic mice. Mol. Biol. Cell 6, 1861–1873 (1995).
29. R. Z. Florkiewicz, A. Baird, A. M. Gonzalez, Multiple forms of bFGF: Differential nuclear and cell surface localization. Growth Factors 4, 265–275 (1991).
30. J. E. Lazarus, A. Hegde, A. C. Andrade, O. Nilsson, J. Baron, Fibroblast growth factor expression in the postnatal growth plate. Bone 40, 577–586 (2007).
31. P. Krejci, D. Krakow, P. B. Mekikian, W. R. Wilcox, Fibroblast growth factors 1, 2, 17, and 19 are the predominant FGF ligands expressed in human fetal growth plate cartilage. Pediatr. Res. 61, 267–272 (2007).
32. M. C. Naski, J. S. Colvin, J. D. Coffin, D. M. Ornitz, Repression of hedgehog signaling and BMP4 expression in growth plate cartilage by fibroblast growth factor receptor 3. Development 125, 4977–4988 (1998).
33. D. K. Waller, A. Correa, T. M. Vo, Y. Wang, C. Hobbs, P. H. Langlois, K. Pearson, P. A. Romitti, G. M. Shaw, J. T. Hecht, The population-based prevalence of achondroplasia and thanatophoric dysplasia in selected regions of the US. Am. J. Med. Genet. A 146A, 2385–2389 (2008).
34. F. Oberklaid, D. M. Danks, F. Jensen, L. Stace, S. Rosshandler, Achondroplasia and hypochondroplasia. Comments on frequency, mutation rate, and radiological features in skull and spine. J. Med. Genet. 16, 140–146 (1979).
35. X. Wen, X. Li, Y. Tang, J. Tang, S. Zhou, Y. Xie, J. Guo, J. Yang, X. Du, N. Su, L. Chen, Chondrocyte FGFR3 regulates bone mass by inhibiting osteogenesis. J. Biol. Chem. 291, 24912–24921 (2016).
36. N. Su, X. Li, Y. Tang, J. Yang, X. Wen, J. Guo, J. Tang, X. Du, L. Chen, Deletion of FGFR3 in osteoclast lineage cells results in increased bone mass in mice by inhibiting osteoclastic bone resorption. J. Bone Miner. Res. 31, 1676–1687 (2016).
37. A. Vidrich, J. M. Buzan, C. Ilo, L. Bradley, K. Skaar, S. M. Cohn, Fibroblast growth factor receptor-3 is expressed in undifferentiated intestinal epithelial cells during murine crypt morphogenesis. Dev. Dyn. 230, 114–123 (2004).
38. Y. Xie, N. Su, M. Jin, H. Qi, J. Yang, C. Li, X. Du, F. Luo, B. Chen, Y. Shen, H. Huang, C. J. Xian, C. Deng, L. Chen, Intermittent PTH (1-34) injection rescues the retarded skeletal development and postnatal lethality of mice mimicking human achondroplasia and thanatophoric dysplasia. Hum. Mol. Genet. 21, 3941–3955 (2012).
39. S. Garcia, B. Dirat, T. Tognacci, N. Rochet, X. Mouska, S. Bonnafous, S. Patouraux, A. Tran, P. Gual, Y. Le Marchand-Brustel, I. Gennero, E. Gouze, Postnatal soluble FGFR3 therapy rescues achondroplasia symptoms and restores bone growth in mice. Sci. Transl. Med. 5, 203ra124 (2013).
40. M. Matsushita, S. Hasegawa, H. Kitoh, K. Mori, B. Ohkawara, A. Yasoda, A. Masuda, N. Ishiguro, K. Ohno, Meclozine promotes longitudinal skeletal growth in transgenic mice with achondroplasia carrying a gain-of-function mutation in the FGFR3 gene. Endocrinology 156, 548–554 (2015).
41. D. Komla-Ebri, E. Dambroise, I. Kramer, C. Benoist-Lasselin, N. Kaci, C. Le Gall, L. Martin, P. Busca, F. Barbault, D. Graus-Porta, A. Munnich, M. Kneissel, F. Di Rocco, M. Biosse-Duplan, L. Legeai-Mallet, Tyrosine kinase inhibitor NVP-BGJ398 functionally improves FGFR3-related dwarfism in mouse model. J. Clin. Invest. 126, 1871–1884 (2016).
42. D. J. Wendt, M. Dvorak-Ewell, S. Bullens, F. Lorget, S. M. Bell, J. Peng, S. Castillo, M. Aoyagi-Scharber, C. A. O'Neill, P. Krejci, W. R. Wilcox, D. L.

Rimoin, S. Bunting, Neutral endopeptidase-resistant C-type natriuretic peptide variant represents a new therapeutic approach for treatment of fibroblast growth factor receptor 3-related dwarfism. J. Pharmacol. Exp. Ther. 353, 132–149 (2015).
43. K. Pejchalova, P. Krejci, W. R. Wilcox, C-natriuretic peptide: An important regulator of cartilage. Mol. Genet. Metab. 92, 210–215 (2007).
44. L. C. Shuhaibar, J. W. Robinson, G. Vigone, N. P. Shuhaibar, J. R. Egbert, V. Baena, T. F. Uliasz, D. Kaback, S.-P. Yee, R. Feil, M. C. Fisher, C. N. Dealy, L. R. Potter, L. A. Jaffe, Dephosphorylation of the NPR2 guanylyl cyclase contributes to inhibition of bone growth by fibroblast growth factor. eLife 6, e31343 (2017).
45. J. W. Robinson, J. R. Egbert, J. Davydova, H. Schmidt, L. A. Jaffe, L. R. Potter, Dephosphorylation is the mechanism of fibroblast growth factor inhibition of guanylyl cyclase-B. Cell. Signal. 40, 222–229 (2017).
46. R. C. Olney, T. C. R. Prickett, E. A. Espiner, W. G. Mackenzie, A. L. Duker, C. Ditro, B. Zabel, T. Hasegawa, H. Kitoh, A. S. Aylsworth, M. B. Bober, C-type natriuretic peptide plasma levels are elevated in subjects with achondroplasia, hypochondroplasia, and thanatophoric dysplasia. J. Clin. Endocrinol. Metab. 100, E355–E359 (2015).
47. F. Lorget, N. Kaci, J. Peng, C. Benoist-Lasselin, E. Mugniery, T. Oppeneer, D. J. Wendt, S. M. Bell, S. Bullens, S. Bunting, L. S. Tsuruda, C. A. O'Neill, F. Di Rocco, A. Munnich, L. Legeai-Mallet, Evaluation of the therapeutic potential of a CNP analog in a FGFR3 mouse model recapitulating achondroplasia. Am. J. Hum. Genet. 91, 1108–1114 (2012).
48. L. Baerts, N. Gomez, M. Vanderheyden, I. De Meester, K. McEntee, Possible mechanisms for brain natriuretic peptide resistance in heart failure with a focus on interspecies differences and canine BNP biology. Vet. J. 194, 34–39 (2012).
49. W. T. Abraham, M. E. Lauwaars, J. K. Kim, R. L. Peñna, R. W. Schrier, Reversal of atrial natriuretic peptide resistance by increasing distal tubular sodium delivery in patients with decompensated cirrhosis. Hepatology 22, 737–743 (1995).
50. X. Zhang, O. A. Ibrahimi, S. K. Olsen, H. Umemori, M. Mohammadi, D. M. Ornitz, Receptor specificity of the fibroblast growth factor family: The complete mammalian FGF family. J. Biol. Chem. 281, 15694–15700 (2006).
51. Z. Liu, K. J. Lavine, I. H. Hung, D. M. Ornitz, FGF18 is required for early chondrocyte proliferation, hypertrophy and vascular invasion of the growth plate. Dev. Biol. 302, 80–91 (2007).
52. I. H. Hung, K. Yu, K. J. Lavine, D. M. Ornitz, FGF9 regulates early hypertrophic chondrocyte differentiation and skeletal vascularization in the developing stylopod. Dev. Biol. 307, 300–313 (2007).
53. X.-L. Wu, M.-M. Gu, L. Huang, X.-S. Liu, H.-X. Zhang, X.-Y. Ding, J.-Q. Xu, B. Cui, L. Wang, S.-Y. Lu, X.-Y. Chen, H.-G. Zhang, W. Huang, W.-T. Yuan, J.-M. Yang, Q. Gu, J. Fei, Z. Chen, Z.-M. Yuan, Z.-G. Wang, Multiple synostoses syndrome is due to a missense mutation in exon 2 of FGF9 gene. Am. J. Hum. Genet. 85, 53–63 (2009).
54. I. Gudernova, S. Foldynova-Trantirkova, B. El Ghannamova, B. Fafilek, M. Varecha, L. Balek, E. Hruba, L. Jonatova, I. Jelinkova, M. K. Bosakova, L. Trantirek, J. Mayer, P. Krejci, One reporter for in-cell activity profiling of majority of protein kinase oncogenes. eLife 6, e21536 (2017).
55. V. V. Mossine, J. K. Waters, M. Hannink, T. P. Mawhinney, PiggyBac transposon plus insulators overcome epigenetic silencing to provide for stable signaling pathway reporter cell lines. PLOS ONE 8, e85494 (2013).

56. A. Prader, R. H. Largo, L. Molinari, C. Issler, Physical growth of Swiss children from birth to 20 years of age. First Zurich longitudinal study of growth and development. Helv. Paediatr. Acta Suppl. 52, 1–125 (1989).
57. J. Hoover-Fong, J. McGready, K. Schulze, A. Y. Alade, C. I. Scott, A height-for-age growth reference for children with achondroplasia: Expanded applications and comparison with original reference data. Am. J. Med. Genet. A 173, 1226–1230 (2017).
58. L. F. Escobar, M. Tucker, M. Bamshad, A second family with CATSHL syndrome: Confirmatory report of another unique FGFR3 syndrome. Am. J. Med. Genet. A 170, 1908–1911 (2016).
59. P. Makrythanasis, S. Temtamy, M. S. Aglan, G. A. Otaify, H. Hamamy, S. E. Antonarakis, A novel homozygous mutation in FGFR3 causes tall stature, severe lateral tibial deviation, scoliosis, hearing impairment, camptodactyly, and arachnodactyly. Hum. Mutat. 35, 959–963 (2014).
60. K. Okita, Y. Matsumura, Y. Sato, A. Okada, A. Morizane, S. Okamoto, H. Hong, M. Nakagawa, K. Tanabe, K. Tezuka, T. Shibata, T. Kunisada, M. Takahashi, J. Takahashi, H. Saji, S. Yamanaka, A more efficient method to generate integration-free human iPS cells. Nat. Methods 8, 409–412 (2011).
61. S. Eto, M. Goto, M. Soga, Y. Kaneko, Y. Uehara, H. Mizuta, T. Era, Mesenchymal stem cells derived from human iPS cells via mesoderm and neuroepithelium have different features and therapeutic potentials. PLOS ONE 13, e0200790 (2018).
62. A. Yamashita, M. Morioka, Y. Yahara, M. Okada, T. Kobayashi, S. Kuriyama, S. Matsuda, N. Tsumaki, Generation of scaffoldless hyaline cartilaginous tissue from human iPSCs. Stem Cell Rep. 4, 404–418 (2015).

Acknowledgments: We thank Y. Nakano, Osaka University Graduate School of Medicine, for technical assistance; V. V. Mossine, Department of Biochemistry, University of Missouri, for donation of TR01F plasmid; H. Verescakova, Institute of Biophysics, Czech Academy of Sciences, for ReACH Registry data acquisition; and I. Gudernova and L. Balek, Masaryk University, and J. Martin, University of California Los Angeles, for excellent technical assistance. We also thank TransGenic Inc. for their contributions to transgenic mice manipulations and pharmacological studies based on the contract research.

Funding: This study was supported by the Japan Agency for Medical Research and Development (AMED); the Ministry of Education, Youth and Sports of the Czech Republic (National Program of Sustainability II projects LQ1605 and LQ1601; LTAUSA19030; CZ.02.1.01/0.0/0.0/15_003/0000460); the Agency for Healthcare Research of the Czech Republic (NV18-08-00567); and the Czech Science Foundation (GA17-09525S and GA19-20123S).

Author contributions: T.Ki., M.Bo., Y.No., K.Y., S.F., F.C., I.D., T.Ku., M.P., M.F., B.F., E.H., T.G., S.P.A., R.G., M.Bu., M.K., T.Z., J.K., and D.K. designed and performed experiments and acquired and analyzed data. S.B. performed mathematical modeling. Y.Na., K.O., and P.K. designed experiments and interpreted data. Y.Na., K.O., D.K., and P.K. obtained funding. P.K., Y.Na., and K.O. wrote the manuscript, with contributions from the other authors.

Competing interests: Y.No., S.F., M.F., and Y.Na. are employees of RIBOMIC Inc. P.K. is under a paid consultant contract with RIBOMIC Inc. The other authors declare that they have no competing interests.

Data and materials availability: All data associated with this study are present in the paper or the Supplementary Materials. RBM-007 is a product of RIBOMIC Inc. and is available under a material transfer agreement.

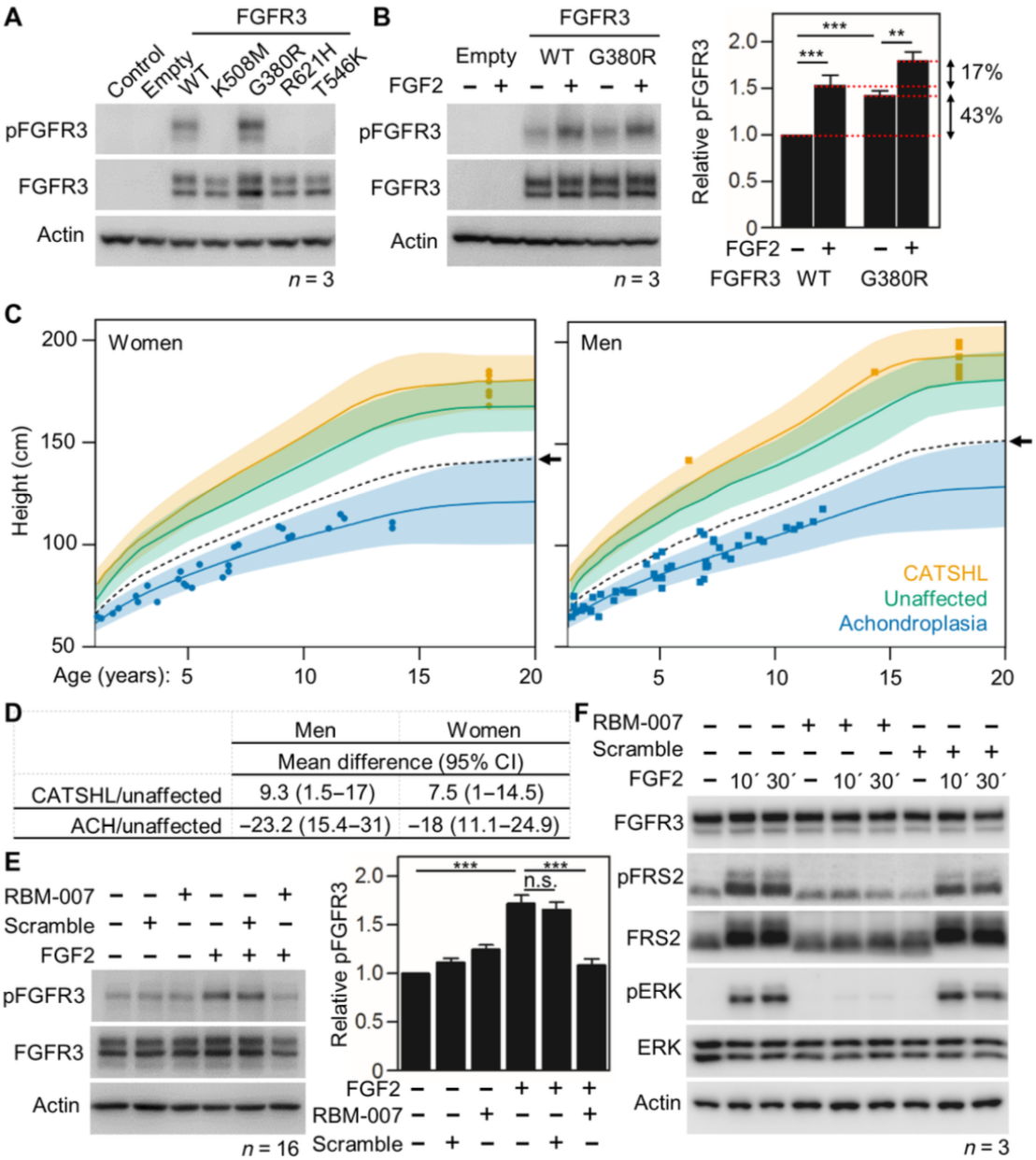
A
FGFR3
Control
Empty
WT
K508M
G380R
R621H
T546K
pFGFR3
FGFR3
Actin
n = 3
B
FGFR3
Empty
WT
G380R
FGF2 – + – + – +
pFGFR3
FGFR3
Actin
n = 3
Relative pFGFR3
2.0
1.5
1.0
0.5
0
***
***
**
17%
43%
FGF2 – + – +
FGFR3 WT G380R
C
Women
Men
Height (cm)
200
150
100
50
Age (years): 5 10 15 20
CATSHL
Unaffected
Achondroplasia
D
Men
Women
Mean difference (95% CI)
CATSHL/unaffected
9.3 (1.5–17)
7.5 (1–14.5)
ACH/unaffected
–23.2 (15.4–31)
–18 (11.1–24.9)
E
RBM-007 – – + – – +
Scramble – + – – + –
FGF2 – – – + + +
pFGFR3
FGFR3
Actin
n = 16
Relative pFGFR3
2.0
1.5
1.0
0.5
0
***
***
n.s.
FGF2 – – – + + +
RBM-007 – – + – – +
Scramble – + – – + –
F
RBM-007 – – – + + + – – –
Scramble – – – – – – + + +
FGF2 – 10′ 30′ – 10′ 30′ – 10′ 30′
FGFR3
pFRS2
FRS2
pERK
ERK
Actin
n = 3

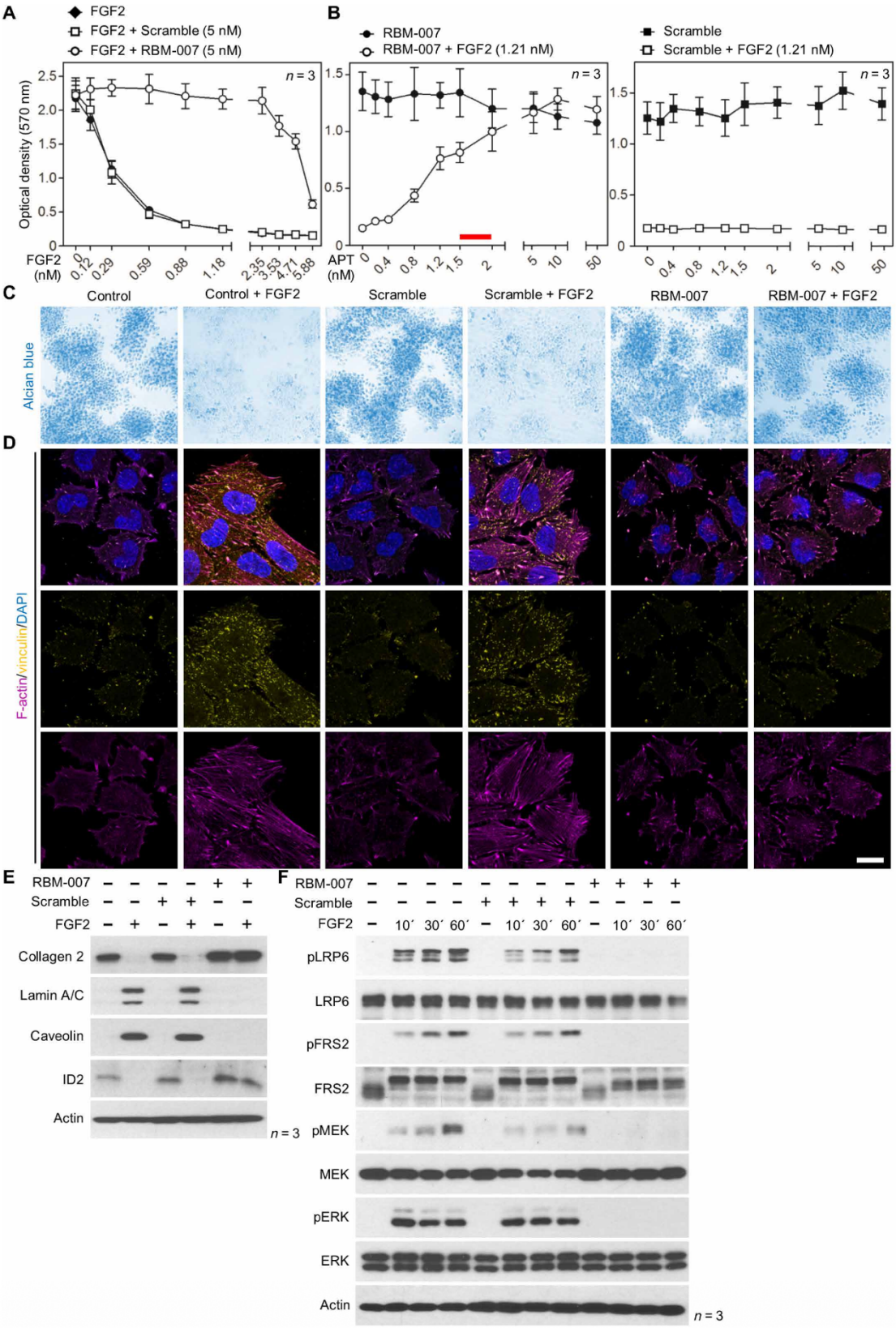
A
FGF2
FGF2 + Scramble (5 nM)
FGF2 + RBM-007 (5 nM)
Optical density (570 nm)
n = 3
FGF2 (nM)
0 0.12 0.29 0.59 0.88 1.18 2.35 3.53 4.71 5.88
B
RBM-007
RBM-007 + FGF2 (1.21 nM)
Scramble
Scramble + FGF2 (1.21 nM)
n = 3
APT (nM)
0 0.4 0.8 1.2 1.5 2 5 10 50
C
Control
Control + FGF2
Scramble
Scramble + FGF2
RBM-007
RBM-007 + FGF2
Alcian blue
D
F-actin/vinculin/DAPI
E
RBM-007
Scramble
FGF2
Collagen 2
Lamin A/C
Caveolin
ID2
Actin
n = 3
F
RBM-007
Scramble
FGF2
10′ 30′ 60′
pLRP6
LRP6
pFRS2
FRS2
pMEK
MEK
pERK
ERK
Actin
n = 3

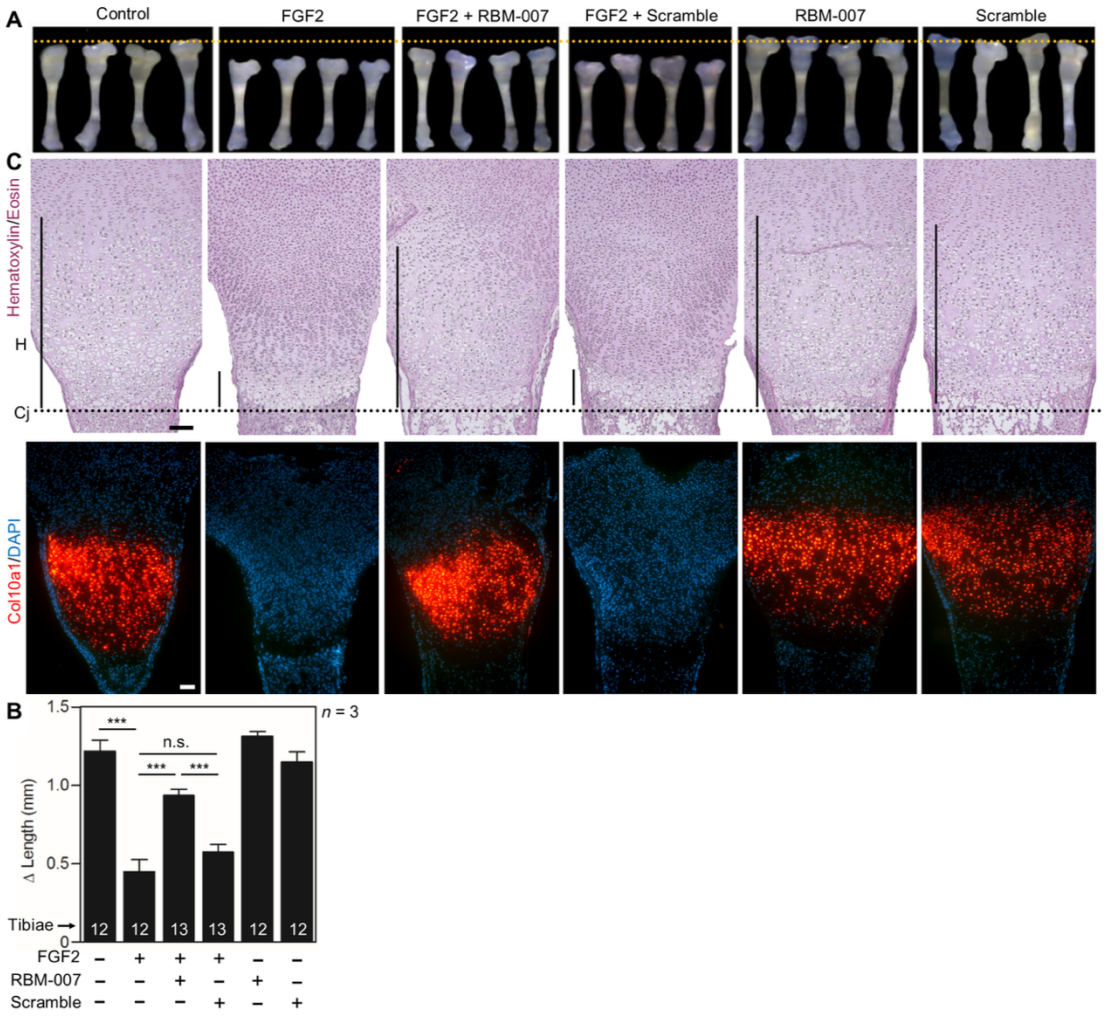
A
Control
FGF2
FGF2 + RBM-007
FGF2 + Scramble
RBM-007
Scramble
C
Hematoxylin/Eosin
H
Cj
Col10a1/DAPI
B
n = 3
***
n.s.
***
***
Δ Length (mm)
1.5
1.0
0.5
0
Tibiae
12
12
13
13
12
12
FGF2 – + + + – –
RBM-007 – – + – + –
Scramble – – – + – +

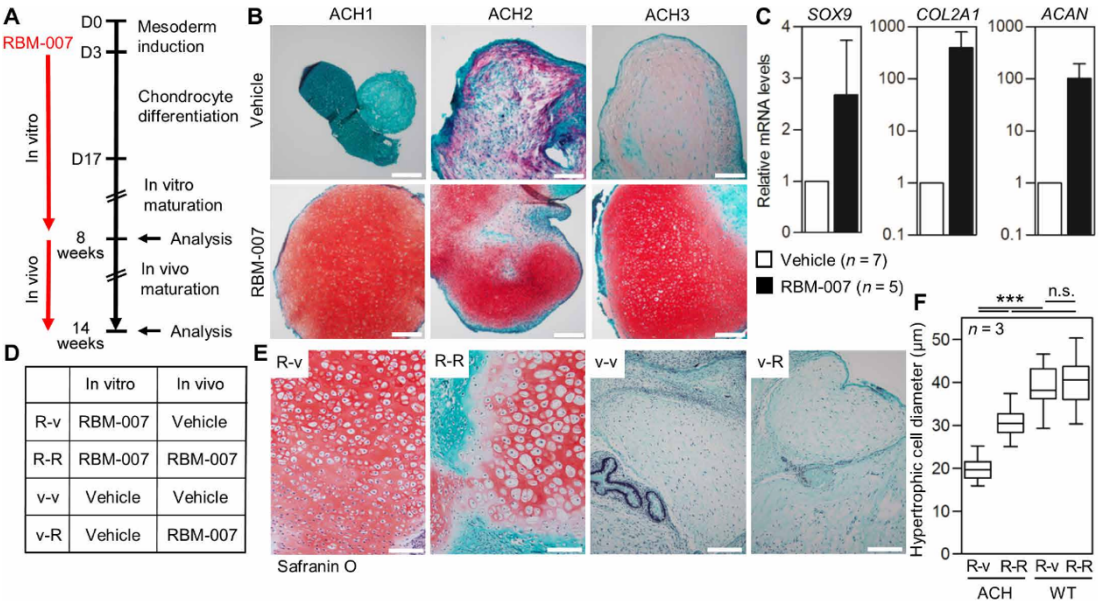
A
RBM-007
In vitro
In vivo
D0
D3
D17
8 weeks
14 weeks
Mesoderm induction
Chondrocyte differentiation
In vitro maturation
Analysis
In vivo maturation
Analysis
B
ACH1
ACH2
ACH3
Vehicle
RBM-007
C
SOX9
COL2A1
ACAN
Relative mRNA levels
Vehicle (n = 7)
RBM-007 (n = 5)
D
In vitro
In vivo
R-v
RBM-007
Vehicle
R-R
RBM-007
RBM-007
v-v
Vehicle
Vehicle
v-R
Vehicle
RBM-007
E
R-v
R-R
v-v
v-R
Safranin O
F
***
n.s.
n = 3
Hypertrophic cell diameter (μm)
R-v R-R R-v R-R
ACH
WT

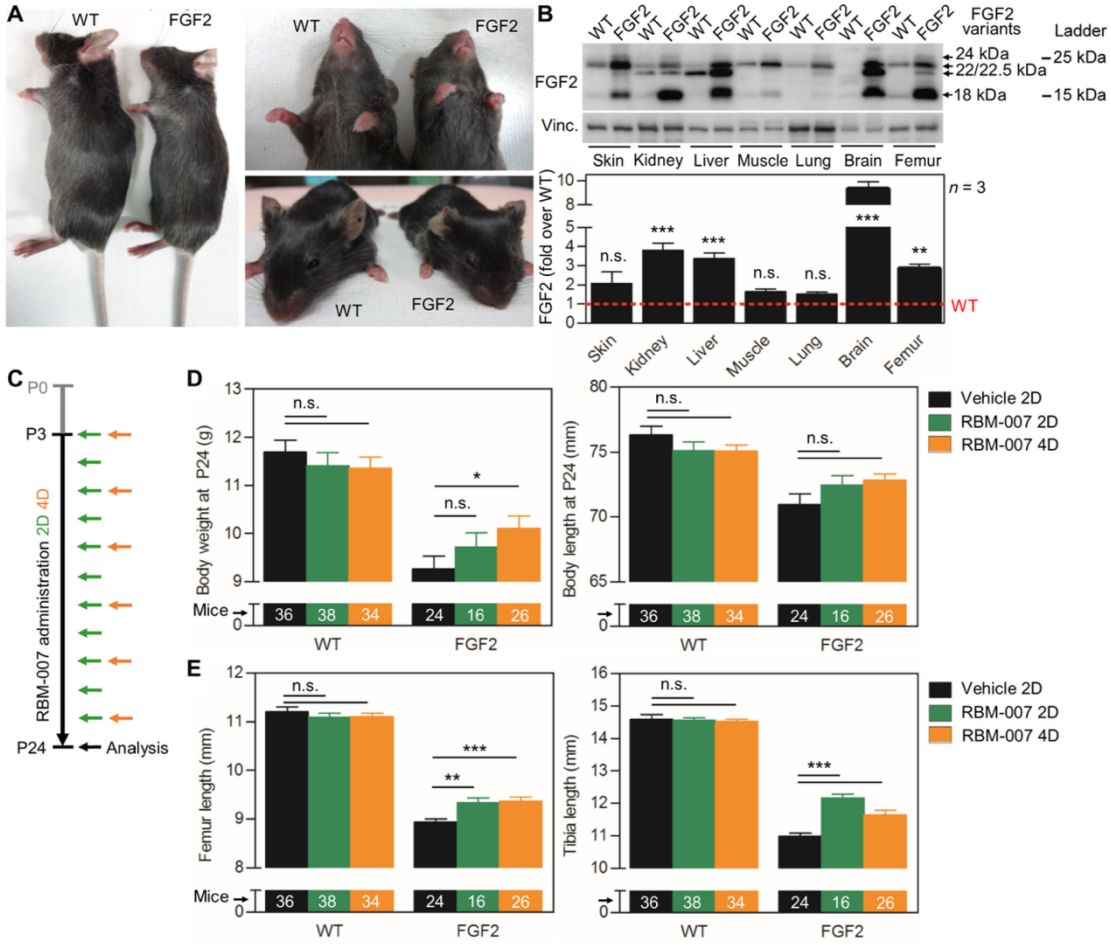
A
WT
FGF2
WT
FGF2
WT
FGF2
B
WT FGF2 WT FGF2 WT FGF2 WT FGF2 WT FGF2 WT FGF2 WT FGF2
FGF2 variants
Ladder
FGF2
24 kDa
22/22.5 kDa
18 kDa
25 kDa
15 kDa
Vinc.
Skin Kidney Liver Muscle Lung Brain Femur
FGF2 (fold over WT)
n = 3
n.s.
***
***
n.s.
n.s.
***
**
WT
Skin Kidney Liver Muscle Lung Brain Femur
C
P0
P3
RBM-007 administration 2D 4D
P24
Analysis
D
Body weight at P24 (g)
n.s.
n.s.
*
Mice
36 38 34 24 16 26
WT
FGF2
Body length at P24 (mm)
n.s.
n.s.
Vehicle 2D
RBM-007 2D
RBM-007 4D
E
Femur length (mm)
n.s.
**
***
Tibia length (mm)
n.s.
***

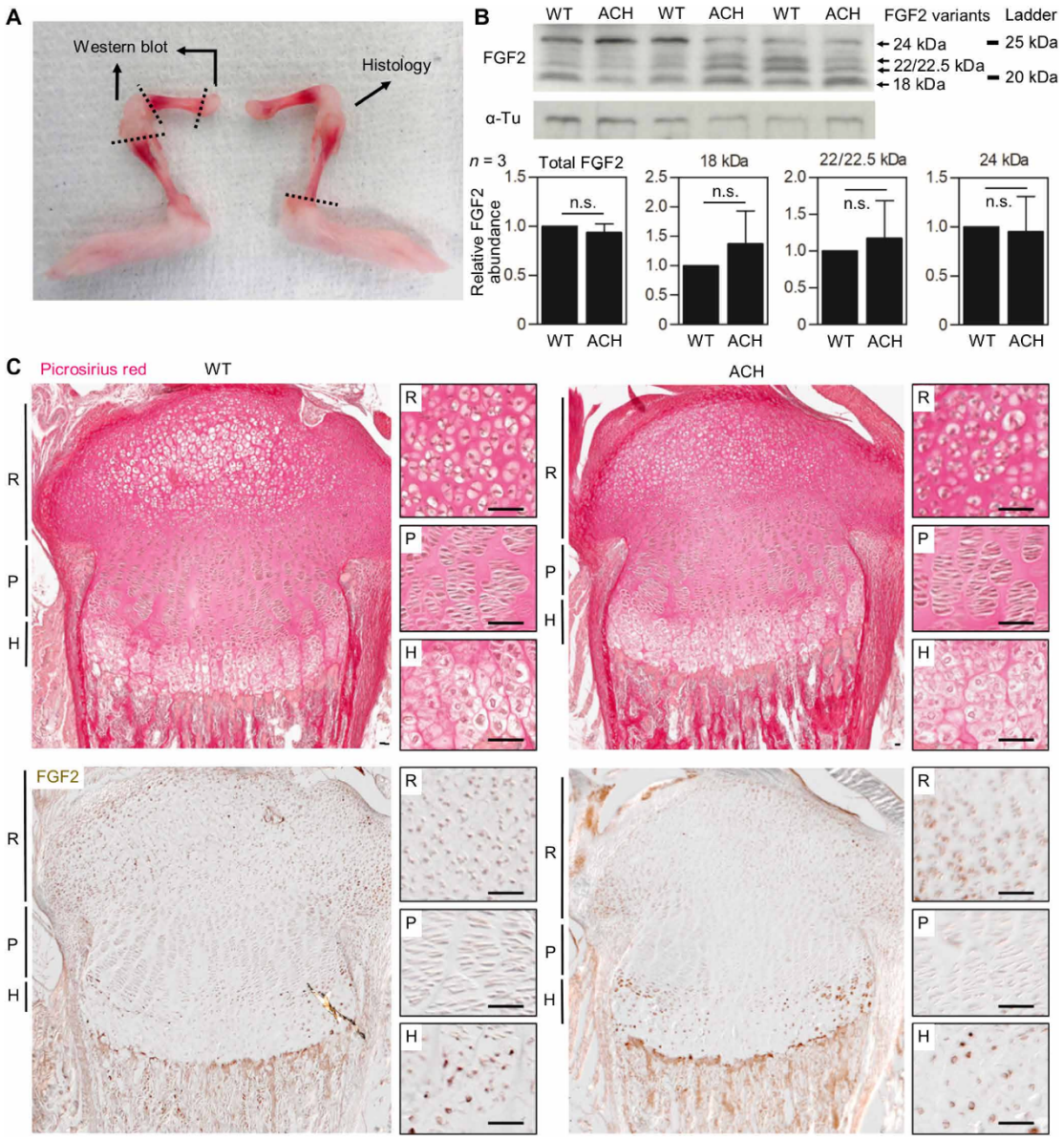
A
Western blot
Histology
B
WT ACH WT ACH WT ACH
FGF2 variants
Ladder
FGF2
α-Tu
24 kDa
22/22.5 kDa
18 kDa
25 kDa
20 kDa
n = 3
Total FGF2
18 kDa
22/22.5 kDa
24 kDa
Relative FGF2 abundance
n.s.
WT ACH
C
Picrosirius red
WT
ACH
R
P
H
FGF2

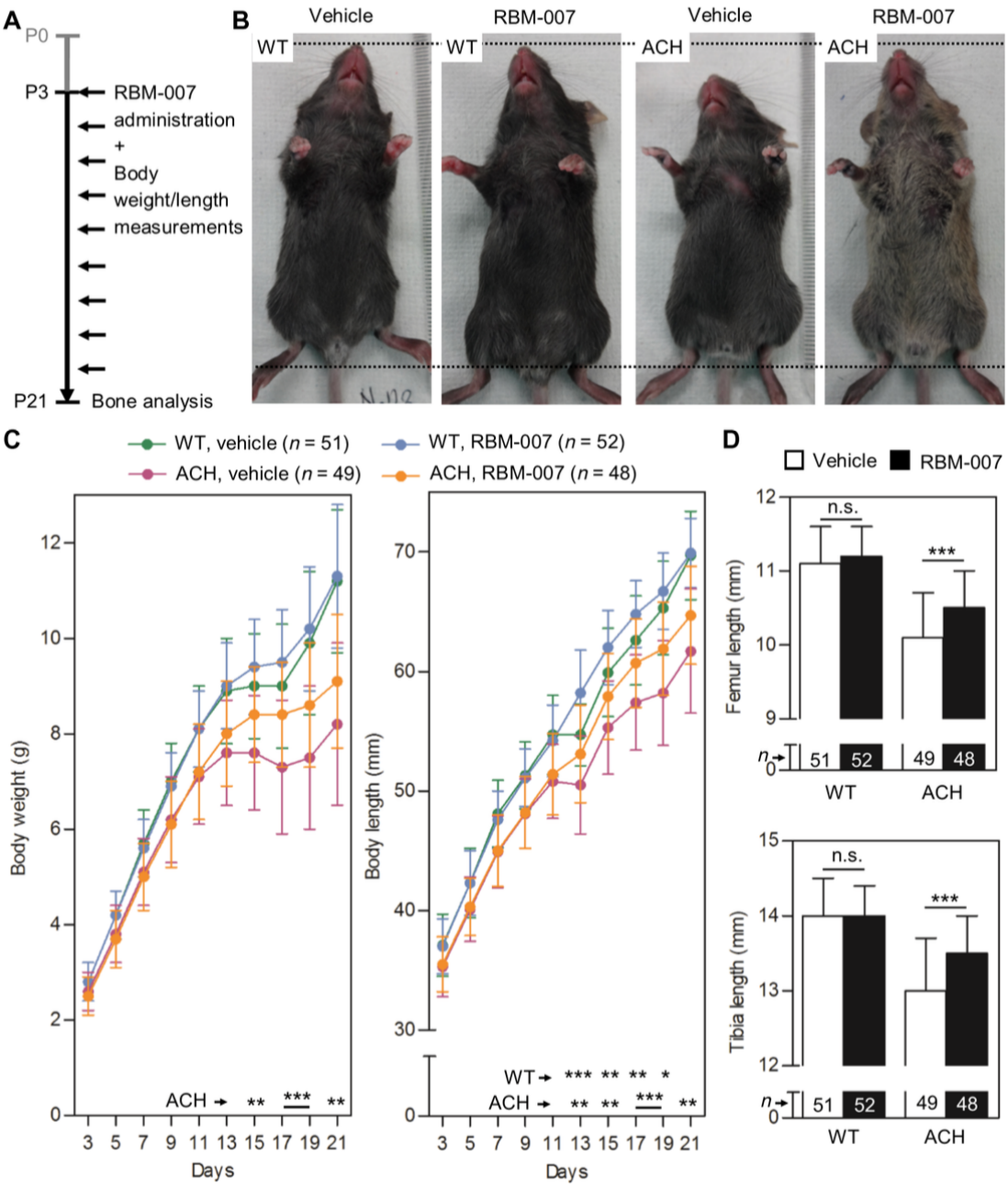
A
P0
P3
RBM-007
administration
+
Body
weight/length
measurements
P21
Bone analysis
B
Vehicle
RBM-007
Vehicle
RBM-007
WT
WT
ACH
ACH
C
WT, vehicle (n = 51)
WT, RBM-007 (n = 52)
ACH, vehicle (n = 49)
ACH, RBM-007 (n = 48)
Body weight (g)
Body length (mm)
Days
Days
ACH
WT
D
Vehicle
RBM-007
Femur length (mm)
Tibia length (mm)
n.s.
***
51
52
49
48
WT
ACH

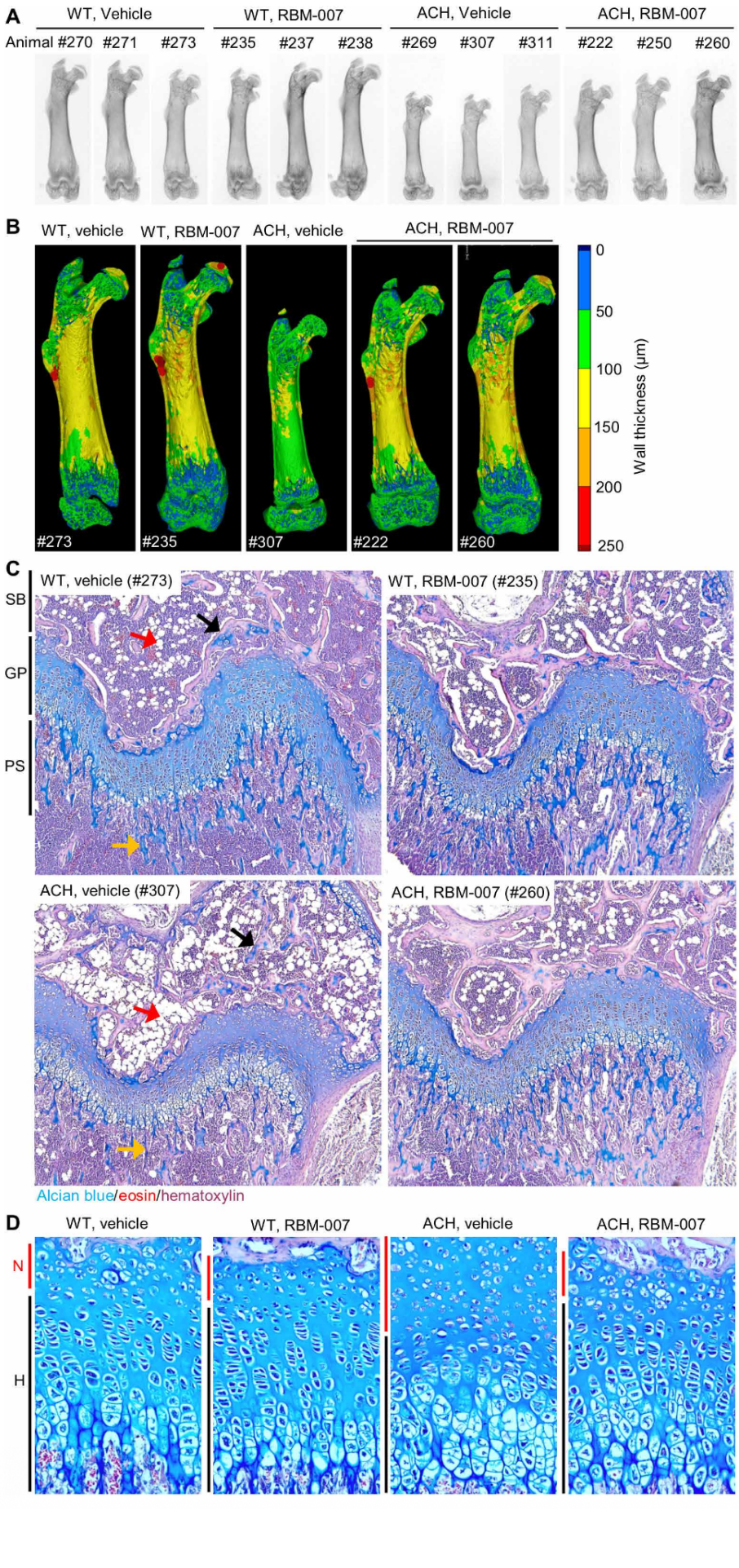
A
WT, Vehicle
WT, RBM-007
ACH, Vehicle
ACH, RBM-007
Animal #270 #271 #273 #235 #237 #238 #269 #307 #311 #222 #250 #260
B
WT, vehicle
WT, RBM-007
ACH, vehicle
ACH, RBM-007
#273
#235
#307
#222
#260
0
50
100
150
200
250
Wall thickness (μm)
C
SB
GP
PS
WT, vehicle (#273)
WT, RBM-007 (#235)
ACH, vehicle (#307)
ACH, RBM-007 (#260)
Alcian blue/eosin/hematoxylin
D
WT, vehicle
WT, RBM-007
ACH, vehicle
ACH, RBM-007
N
H

FIGURE LEGENDS

Fig. 1. RBM-007 inhibits FGF2-mediated activation of FGFR3. (A) MCF7 cells were transfected with C-terminally V5-tagged wild-type (WT) FGFR3 or FGFR3 mutants associated with ACH (G380R) and CATSHL (R621H, T546K), grown for 24 hours, and analyzed for FGFR3 autophosphorylation (p) by Western blot. Kinase-dead mutant K508M serves as negative control for FGFR3 activity. Actin serves as loading control.

(B) MCF7 cells expressing WT FGFR3 and FGFR3-G380R were treated with FGF2 (50 ng/ml) for 2 hours and analyzed for pFGFR3. Integrated optical density was determined (graph). Double-sided arrows indicate the G380R effect on basal and FGF2-mediated activation of FGFR3. Data represent averages from four measurements of three independent experiments. Statistically significant differences are indicated (one-way ANOVA with Bonferroni's correction; $^{**}P < 0.01$, $^{***}P < 0.001$) (mean ± SE).

(C) Growth curves for individuals with CATSHL (n = 8 women, n = 10 men) and ACH (n = 28 women, n = 48 men) compared to non-CATSHL and non-ACH individuals. Data are shown as averages with 95% CI. Dots represent individual patients. Data were obtained from published literature for CATSHL and from ReACH Registry for ACH. Arrows and dashed lines, estimated gain in height in ACH caused by 20 to 30% inhibition of FGFR3-G380R activity.

(D) Growth rate calculations in CATSHL and ACH compared to unaffected individuals.

(E) MCF7 cells were transfected with FGFR3-G380R, grown for 24 hours, treated with FGF2 and RBM-007 for 2 hours, and analyzed for pFGFR3. Blots are representative of 16 independent experiments.

(F) RCSACH cells were treated with 5 nM RBM-007/scramble aptamer and 1.18 nM FGF2 as indicated, and the cell lysates were immunoblotted for pFRS2 and pERK to test the activation of FGFR signaling; actin served as loading control. Data are representative of three independent experiments.

Fig. 2. RBM-007 inhibits FGFR3 signaling in cultured chondrocytes. RCS chondrocytes were treated with (A) 5 nM RBM-007 together with increasing concentrations of FGF2 or (B) 1.21 nM FGF2 together with increasing concentrations of RBM-007 or scramble aptamer. Cell proliferation was assessed 96 hours later by crystal violet assay. Data show means from eight wells with SD and are representative of three independent experiments.

(C and D) Cells were treated with 2.5 nM RBM-007 together with 0.59 nM FGF2. Three days later, sulfated proteoglycan matrix was stained by Alcian blue (C), and F-actin stress fibers and focal adhesions were stained by phalloidin–Alexa Fluor 594 and vinculin-FITC, respectively (D); nuclei were counterstained by DAPI. Scale bar, 20 μm. The images are representative of three independent experiments.

(E and F) RCS cells were treated with 10 nM (E) or 5 nM (F) RBM-007 together with 1.18 nM of FGF2 for 48 hours (E) or 10 to 60 min (F). Cell lysates were immunoblotted for (E) collagen type 2, lamin A/C, caveolin, and ID2 to demonstrate the FGF2-induced premature senescence, and (F) pLRP6, FRS2, MEK, and ERK to test the activation of

FGFR signaling; actin and total amounts of proteins served as loading controls. Data are representative of three independent experiments.

Fig. 3. RBM-007 restores impaired chondrocyte differentiation in murine tibia organ culture. E18 tibiae were cultured in media supplemented with FGF2 (100 ng/ml) and 100 nM RBM-007 or scramble aptamer for 8 days.

(A) Overall appearance of the tibiae at the end of the experiment. The dotted line indicates length of an average nontreated control tibia. The images are representative of three independent experiments, each consisting of four to five tibiae in each group.

(B) Differences of tibia length before and after the 8-day cultivation (Δ length) (mean ± SE). Statistically significant differences are indicated (one-way ANOVA with Bonferroni's correction; ***$P < 0.001$; n.s., not significant).

(C) Histological sections of representative tibiae stained with hematoxylin and eosin with the indicated hypertrophic zone (H; top), which is also detected using Col10a1 RNAscope (bottom). Scale bars, 100 μm. Cj, chondro-osseous junction.

Fig. 4. RBM-007 restores inhibition of ACH chondrocyte differentiation in vitro and in vivo.

(A) Mesoderm was induced in feeder-free hiPSC for 3 days, followed by chondrogenic differentiation (14 days) and maturation of the chondrocytic bodies (5.5 weeks). Eight-week-old chondrocytic bodies were implanted subcutaneously to the C.B-17/lcr-scid/scidJcl mice and allowed to mature for an additional 6 weeks. RBM-007 (100 nM) was present through the differentiation and maturation periods.

(B) Sections of the 8-week-old chondrocytic bodies stained by Safranin O; red, mature cartilage; blue, immature cartilage. RBM-007 rescued the ACH-driven inhibition of the chondrocytic maturation of three ACH hiPSC cell lines used (ACH1 to ACH3). Scale bars, 200 μm.

(C) Expression of SOX9, COL2A1, and ACAN in 8-week-old ACH chondrocytic bodies using qRT-PCR. RBM-007 increased expression of all markers compared to vehicle control. Bars show compilation of data obtained from ACH1 to ACH3 hiPSC lines, in total five colonies treated with RBM-007 and seven treated with the vehicle (mean ± SE).

(D) Scheme of the transplantation experiments.

(E) Histology of ACH2-derived chondrocytic particles stained with Safranin O after 14 weeks of differentiation and maturation. RBM-007 rescued chondrocyte maturation defect only when used during the 8 weeks of in vitro differentiation. Scale bars, 100 μm.

(F) Analysis of chondrocyte hypertrophy and change in chondrocyte diameter in ACH xenografts treated with RBM-007/RBM-007 (R-R) protocol (one-way ANOVA with Bonferroni's correction; ***$P < 0.001$; n.s., not significant). Graph shows compilation of ACH1 to ACH3 hiPSC lines. Ten individual cells were measured in each xenograft; data are representative of three xenografts from three different mice ($n = 3$). Box, first to third quartile; whiskers, minimum to maximum.

Fig. 5. RBM-007 partially rescues bone growth in FGF2-overexpressing mice.

(A) Overall appearance of the FGF2 mice, including shorter body and snout.

(B) Western blot of FGF2 expression in tissues of FGF2-overexpressing mice; vinculin (Vinc.) served as loading control. Signal obtained from three animals (n = 3) and two measurements of each was quantified and plotted. Statistically significant differences are indicated (one-way ANOVA with Dunnett's correction; *P < 0.05, **P < 0.01, ***P < 0.001; n.s., not significant). The dashed red line indicates endogenous FGF2 expression in WT animals.

(C) Scheme of RBM-007 administration and analyses.

(D) Body weight and length were measured at P24 and plotted (mean ± SE).

(E) Femur and tibia lengths were measured at P24 and plotted (mean ± SE). Statistically significant differences are indicated (one-way ANOVA with Dunnett's correction; *P < 0.05, **P < 0.01, ***P < 0.001; n.s., not significant). The number of mice in each group is indicated; n = 36 (WT, vehicle 2D), n = 38 (WT, RBM-007 2D), n = 34 (WT, RBM-007 4D), n = 24 (FGF2, vehicle 2D), n = 16 (FGF2, RBM-007 2D), and n = 26 (FGF2, RBM-007 4D).

Fig. 6. FGF2 expression in the growth plate cartilage of ACH mice.

(A) P7 murine hindlimbs were dissected as indicated and used for Western blotting and histology and immunohistochemistry.

(B) Western blot of FGF2 in growth plate tissue from Fgfr3ACH (ACH) and WT littermates. Arrows indicate different FGF2 protein variants (18, 22/22.5, and 24 kDa). The graphs represent quantification of three replicates of total FGF2 (all bands) or each FGF2 variant (mean ± SE). α-Tubulin (α-Tu) served as loading control and for normalization of FGF2 expression by densitometry (Welch's t test; n.s., not significant). n = 3 animals in each group (WT/ACH).

(C) The WT and ACH growth plates stained by Picrosirius red and anti-FGF2 antibody. Resting (R), proliferative (P), and hypertrophic (H) zones are indicated. Note the widespread expression of FGF2 throughout the growth plate, including perichondrium and perivascular regions. Scale bars, 50 μm. n = 3 animals in each group (WT/ACH).

Fig. 7. RBM-007 restores defective skeletal growth in ACH mice.

(A) Scheme of the RBM-007 administration and analyses.

(B) Overall appearance of WT and ACH mice treated with RMB-007 or vehicle for 18 days, starting at P3.

(C) Body weight and length were measured every other day and plotted (mean ± SD). Statistically significant differences are indicated (Welch's t test; *P < 0.05, **P < 0.01, ***P < 0.001).

(D) Femur and tibia lengths were measured at P21 and plotted (mean ± SD) (Welch's t test; ***P < 0.001; n.s., not significant). n, number of animals and limbs analyzed. n = 51 (WT, vehicle), n = 52 (WT, RBM-007), n = 49 (ACH, vehicle), and n = 48 (ACH, RBM-007).

Fig. 8. RBM-007 restores long bone growth and growth plate morphology in ACH mice.

(A) Overall morphology of femurs in WT and ACH mice treated with RMB-007 or scrambled control aptamer for 18 days (starting at P3), visualized by x-ray tomography. Three femurs from each group were analyzed (n = 3).

(B) Micro-CT imaging of the femurs in 3D; sections in frontal plane through the long axis.

(C) Microstructure of the femoral growth plates (GP) at P21. Black arrow, bony lamellae; red arrow, adipocytes; yellow arrow, mineralized trabeculae. Spongy bone (SB), primary spongiosa (PS).

(D) Microscopic structure of the growth plate cartilage. Nonhypertrophic zone (N) and prehypertrophic and hypertrophic zones (H). Effect of RBM-007 on defective growth plate architecture in ACH mice.